Fermi National Accelerator Laboratory

Fermilab-Pub-91/64-T
March 1991

Nucleon Compton Scattering in Perturbative QCD

A.S. Kronfeld[1] and B. Nižić[2]

[1]Theoretical Physics Group, Fermi National Accelerator Laboratory,*
P.O. Box 500, Batavia IL 60510, USA

[2]Rudjer Bošković Institute,
P.O. Box 1016, YU-41001 Zagreb, Croatia, Yugoslavia

March 19, 1991

Abstract

We have computed the helicity amplitudes for the reactions $\gamma N \to \gamma N$ (N = p, n) at large momentum transfer to lowest order in perturbative QCD. Our cross section for proton Compton scattering shows good qualitative agreement with experimental data, when the proton is modeled by the Chernyak-Oglobin-Zhitnitsky, King-Sachrajda or Gari-Stefanis distribution amplitude. Discrepancies between our results and previous calculations seem to be due to different treatments of numerical integration around singularities.

*Operated by Universities Research Association Inc. under contract with the United States Department of Energy

1 Introduction

Exclusive processes in photon-hadron collisions offer a wide variety of tests of perturbative QCD. The amplitude for a wide-angle exclusive process is given by the convolution of a distribution amplitude summarizing soft, hadronic physics and a hard-scattering amplitude of collinear, constituent partons [1]. The distribution amplitude cannot be computed in perturbation theory, but, as with the structure function in deep inelastic scattering, it could be measured in lower-energy reactions. Application of the perturbative renormalization group and the convolution with parton scattering amplitudes yield predictions for new processes or at higher energies. No distribution amplitude has been measured yet, for two reasons. First, exclusive cross sections are harder to measure because the cross sections are smaller and the backgrounds are higher. Second, the theoretical calculations are demanding because extremely many Feynman diagrams appear, even in leading order. Consequently, for most exclusive processes higher order theoretical calculations, which are necessary before the distribution amplitude could be measured, have not even been contemplated.

In the long run, only computers will have the patience to work out the amplitudes, and the major challenge for the last few years has been to develop a reliable combination of symbolic and numerical algorithms. Farrar and collaborators [2] have developed several codes for symbolic evaluation of the diagrams contributing to the hard-scattering amplitude. They yield the same results, and they agree with all hard-scattering amplitudes that have been calculated by hand. Hence, one can be confident that these symbolic programs are correct for tree diagrams. However, one must also be certain that the subsequent numerical steps involved are robust. The convolution of the hard-scattering amplitude and the distribution amplitude is a multi-dimensional integral over the momentum fractions of the valence partons. This integral is analogous to a loop integral, except that it uses the distribution amplitude to describe the exchange of any and all soft gluons, rather than the propagator to describe the exchange of a single hard particle. In particular, integrable singularities can arise in certain regions of momentum-fraction space, when internal lines of Feynman diagrams go on mass shell, producing an imaginary part in the amplitude.

In this paper we compute the cross sections for nucleon Compton scattering to lowest order in perturbative QCD. This is the simplest experimentally accessible process in which the momentum-fraction integrals yield an imaginary part. We use the same methods [2] as the symbolic computer programs to evaluate the Feynman diagrams, but we do so by hand. Because the singularities in the momentum-fraction integrals can ambush numerical integration routines, we approach them with great caution. Wherever possible, we integrate singular integrands analytically, a step that a computer-based approach could perform symbolically. The remaining one- and two-dimensional integrals are done using VEGAS [3]; for diagrams in which two and those in which three internal lines can go on shell, poles remain in the domain of numerical integration. We use the technique developed in Ref. [4] to evaluate the principal parts of these integrals. (Reference [4] computed meson pair production in two-photon collisions to one loop, which contains ultraviolet, infrared, collinear and principal part singularities in the loop and momentum-fraction integrals.) In a nutshell, a change of variables maps the twin peaks onto each other in such a way that they cancel locally, rather than globally.

For proton Compton scattering there is wide-angle data [5] with center-of-mass energy-squared $4.6\,\mathrm{GeV}^2 < s < 12.1\,\mathrm{GeV}^2$, where perturbative QCD ought to be applicable. There are other data [6, 7, 8], but those experiments concentrated on lower energies and smaller angles, where the formalism of Ref. [1] does not apply. Below we shall compare our results for the unpolarized cross section to the Tufts-MIT-Cornell experiment [5]. The predictions for polarized cross sections and phase of the amplitude can be verified in ep collisions [9], because Compton scattering with a virtual incident photon also contributes to the reaction $eN \to eN\gamma$. When the electron is deflected through

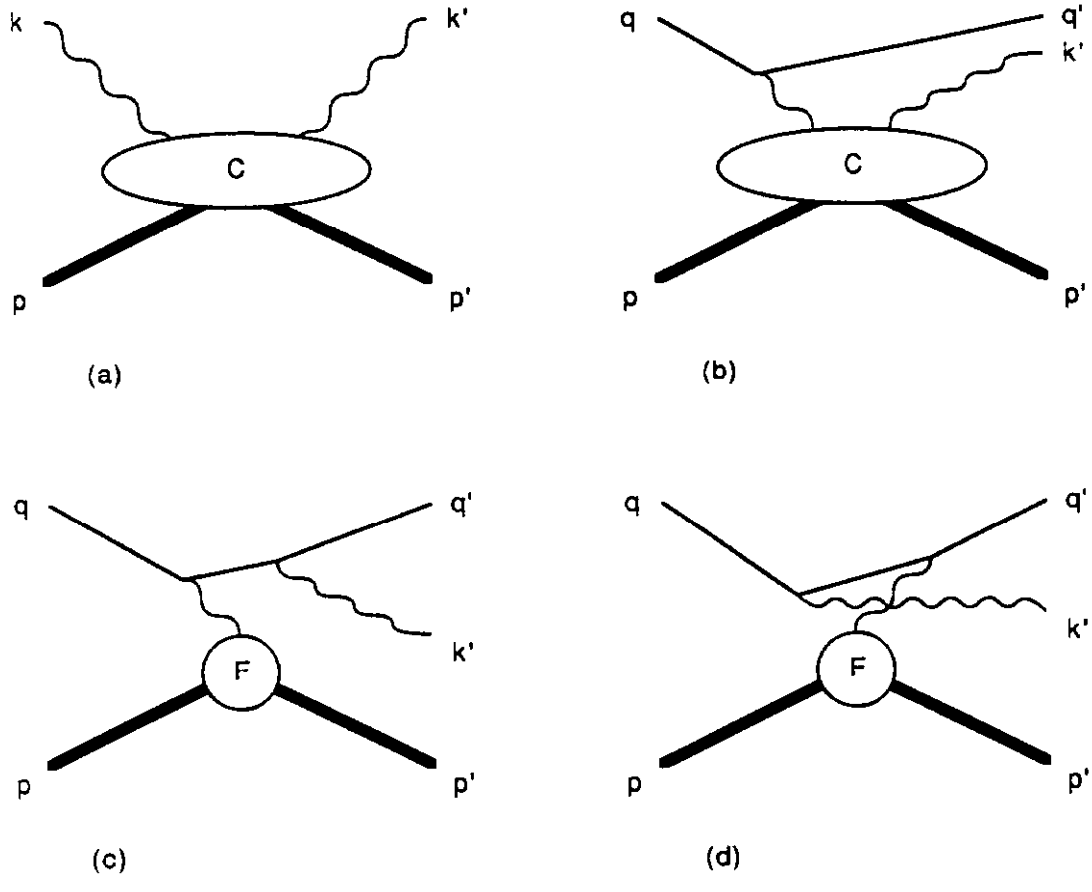

Figure 1: The processes (a) $\gamma N \rightarrow \gamma N$ and (b, c, d) $eN \rightarrow eN\gamma$. The blob labeled C denotes the Compton amplitude, and the one labeled F the electromagnetic form factor.

a small angle, the exchanged photon is almost parallel to it and nearly real, and the Compton sub-process dominates. It may be possible [9] to determine the phase of the Compton amplitude, as a function of the center-of-mass scattering angle, by extracting the interference of the Compton scattering with the sub-processes depicted in Figs. 1(c) and (d). This would be interesting, because the non-zero phase is a non-trivial prediction of perturbative QCD. Moreover, the phase information may provide more stringent constraints on the nucleon distribution amplitude than the cross section alone.

Instead of using data to determine the distribution amplitude, it should be possible to use a non-perturbative QCD calculation. Quenched lattice QCD has so far [10] only produced the first two moments of the nucleon distribution amplitude. There are several calculations of the first *six* moments using QCD sum rules [11, 12, 13]. They agree with each other but only qualitatively with lattice QCD. We will present results using four distribution amplitudes suggested by QCD sum rules [11, 12, 13, 14]. This implies a *de facto* assumption that the higher moments vanish, which may well be unrealistic at accessible values of s.

Two previous attempts [15, 9] to compute nucleon Compton scattering using perturbative QCD have obtained different results, especially for wider center-of-mass scattering angles. Our results disagree with both papers. Reference [9] asserts that the integration scheme of Ref. [15] yields incorrect answers. However, we doubt that the scheme in Ref. [9] is robust. In an example from pion Compton scattering that can be integrated analytically, our method gives the correct result, but the method of Ref. [9] does not. In another example, the contribution of diagram "$A51$" to a specific helicity amplitude, the imaginary part generated by our implementation of the method of Ref. [9] bore no resemblance to our results. And the imaginary part of diagrams like $A51$, in which two internal propagators can go on shell, is a dominant part of the cross section.

This paper is organized as follows: In sect. 2 we discuss the origin of the imaginary part of the Compton amplitude, and explain why the process is dominated by short-distance interactions, even though intermediate quarks or gluons can go on shell. Sect. 3 outlines the details of the calculation. In sect. 4 we compare our results to experiment and discuss theoretical uncertainties. Sect. 5 assesses the potential of future experiments and contains some remarks relevant to the experimental determination of the nucleon distribution amplitude. Finally, there are several technical appendices. The kinematics are set out in Appendix A. Expressions for the Feynman diagrams contributing to the hard-scattering amplitude are tabulated in Appendix B, and an example diagram is worked out in detail in Appendix C. Appendix D reviews our method [4] for performing numerically integrals defined by the principal part prescription.

2 Analytic Structure of Compton Amplitude

An especially interesting aspect of hadron Compton scattering is that perturbative QCD predicts a non-zero imaginary part to the amplitude, even in leading order. There are kinematic regions of momentum-fraction space, in which certain internal quarks or gluons can propagate on the mass shell. One might worry about treating perturbatively such a process. Generally speaking, a freely propagating quark or gluon would be modified by long-distance effects. Consider, however, the space-time diagram of a typical Feynman diagram in pion Compton scattering, depicted in Fig. 2. In this diagram the gluon with momentum $q = xp + k - yp'$ can go on shell when $x(1 - ys^2) - yc^2 = 0$, where $s = \sin(\frac{1}{2}\theta)$, $c = \cos(\frac{1}{2}\theta)$, and θ is the center-of-mass scattering angle. But in that case its three-momentum points in a direction that separates the quark and anti-quark [16]. In our conventions, the scattering takes place in the XZ plane, near the origin, with the outgoing hadron moving towards $X > 0$. (X and Z are spatial coordinates.) But when $q^2 = 0$ one finds $q_X < 0$.

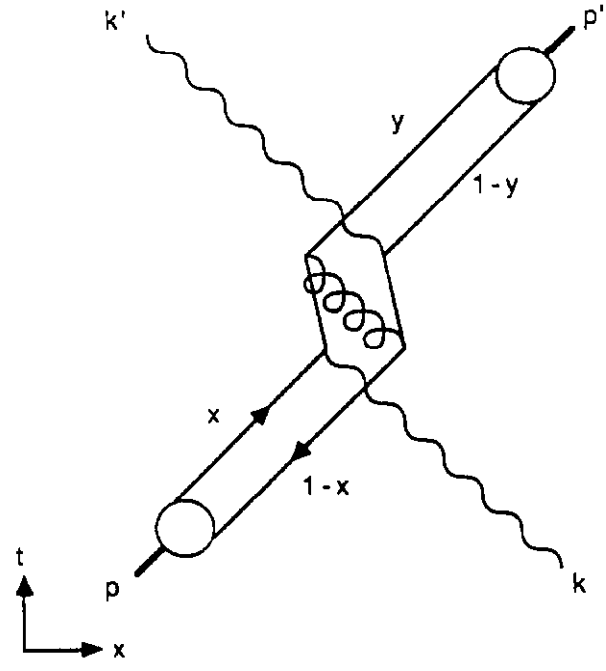

Figure 2: Space-time diagram of a Feynman diagram with an internal gluon on mass shell. When the gluon propagates a short distance, as shown, the pion can re-form. If the gluon propagated ten times further, the re-formation probability of the pion would be tiny.

Hence, if the on-shell parton propagates over any significant distance, then the pion has a negligible probability to re-form. The entire exclusive reaction takes place in a small region, despite the gluon's on-shell propagation, and perturbative QCD is applicable. This feature is generic: internal on-shell partons always tend to tear the hadron apart, decreasing the likelihood that the process indeed be an exclusive one.

A related question is whether the imaginary part is reliably estimated by low-order perturbation theory, or whether Sudakov corrections must be re-summed. Fortunately, the former is the case [17]. The essential point is that the singularities do not pinch. In a higher order correction, the quark momenta will be off shell, by an amount λ^2, before emitting the parton that can go on shell. The position of the pole in momentum-fraction space is shifted by $O(\lambda^2/E^2)$, where E is a hard momentum flowing the Feynman diagram. Since the contour is not pinched, it can move to accommodate the shift. As a result, soft contributions produce only negligible effects of $O(\lambda^2/E^2)$, rather than large Sudakov logarithms $O(\log(E^2/\lambda^2))$.

The appearance of an imaginary part at leading order in α_S is a non-trivial prediction of perturbative QCD. It means that the phase of the amplitude need not be small, and that only a complete calculation can predict it. It would be surprising if the phase were small for all scattering angles; indeed it would impose strong constraints on the form of the nucleon distribution amplitude.

3 Details of the Calculation

The process $\gamma N \to \gamma N$ (N = p, n) is described by the helicity amplitudes $\mathcal{M}^{\lambda\lambda'}_{hh'}(s,t)$, where h (h') is the initial (final) nucleon helicity and λ (λ') is the initial (final) photon helicity. Symmetries

impose some relations among the amplitudes: Parity invariance implies

$$\mathcal{M}^{\lambda\lambda'}_{hh'}(s,t) = \mathcal{M}^{\bar{\lambda}\bar{\lambda}'}_{\bar{h}\bar{h}'}(s,t), \tag{3.1}$$

where the bar denotes opposite helicity, and time-reversal invariance implies

$$\mathcal{M}^{\lambda\lambda'}_{hh'}(s,t) = \mathcal{M}^{\lambda'\lambda}_{h'h}(s,t). \tag{3.2}$$

In the course of calculating $\mathcal{M}^{\lambda\lambda'}_{hh'}(s,t)$ it turns out that Eq. (3.1) is best viewed as a labor-saving device, but Eq. (3.2) is best implemented as a check.

In perturbative QCD the helicity amplitude is given by

$$\mathcal{M}^{\lambda\lambda'}_{hh'}(s,t) = \sum_{d,i} \int [dx][dy]\, \phi_i(x_1,x_2,x_3) T_i^{(d)}(x,h,\lambda;y,h',\lambda') \phi_i^*(y_1,y_2,y_3). \tag{3.3}$$

Here $\phi_i(x_1,x_2,x_3)$ is the distribution amplitude for the i-th Fock state in the nucleon. This paper works in the leading twist approximation, in which only the valence Fock states contribute. For the nucleon there are three spin-flavor combinations; cf. Eq. (3.7). The hard-scattering amplitude from diagram d of the three collinear quarks with the photons, $T_i^{(d)}(x,h,\lambda;y,h',\lambda')$, factors into

$$T_i^{(d)}(x,h,\lambda;y,h',\lambda') = C^{(d)} g^4\, Z_i^{(d)} \tilde{T}^{(d)}(x,h,\lambda;y,h',\lambda'), \tag{3.4}$$

where $C^{(d)}$ is the SU(N) color factor, g is the QCD coupling constant, $Z_i^{(d)}$ is the product of the electric charges of the struck quarks, and $\tilde{T}^{(d)}(x,h,\lambda;y,h',\lambda')$ is a color- and flavor-independent factor containing propagators and spin information. In the description of the calculation, when we write "hard-scattering amplitude" we frequently mean $\tilde{T}^{(d)}(x,h,\lambda;y,h',\lambda')$.

Because QED and QCD are vector gauge theories, the amplitudes for which $h \neq h'$ are proportional to the (quark or nucleon) mass. At high energies they are therefore suppressed, and in the leading twist approximation they should be ignored. Combining this observation with Eqs. (3.1) and (3.2) one finds that there are eight non-negligible helicity amplitudes, of which only three are independent. We shall take

$$\mathcal{M}^{\uparrow\uparrow}_{\uparrow\uparrow}(s,t), \quad \mathcal{M}^{\uparrow\downarrow}_{\uparrow\uparrow}(s,t), \text{ and } \mathcal{M}^{\downarrow\downarrow}_{\uparrow\uparrow}(s,t) \tag{3.5}$$

to be the independent set and present results for these helicity combinations in sec. 4.

3.1 Distribution amplitude

The most general state of collinear quarks with proton quantum numbers and helicity $h = +1$ is

$$|p_\uparrow\rangle = \frac{f_N}{8\sqrt{6}} \int [dx] \sum_i \phi_i(x_1,x_2,x_3)\, |i;x_1,x_2,x_3\rangle, \tag{3.6}$$

where f_N is a constant, to be determined in a non-perturbative calculation or from experiment. The measure for the quark momentum fractions is $[dx] = dx_1 dx_2 dx_3 \delta(1-x_1-x_2-x_3)$. The spin-flavor states are

$$\begin{aligned} |1;x_1,x_2,x_3\rangle &= |u_\uparrow(x_1) u_\downarrow(x_2) d_\uparrow(x_3)\rangle, \\ |2;x_1,x_2,x_3\rangle &= |u_\uparrow(x_1) d_\downarrow(x_2) u_\uparrow(x_3)\rangle, \\ |3;x_1,x_2,x_3\rangle &= |d_\uparrow(x_1) u_\downarrow(x_2) u_\uparrow(x_3)\rangle; \end{aligned} \tag{3.7}$$

Table 1: Coefficients of distribution amplitude ϕ_1 in several models based on QCD sum rules.

model	CZ	COZ	KS	GS
Ref.	[11]	[12]	[13]	[14]
1	1.69	5.880	8.40	6.040
x_1	−9.26	−25.956	−26.88	−16.775
x_3	−10.94	−20.076	−35.28	−34.985
x_1^2	22.70	36.792	35.28	−1.027
x_3^2	13.45	19.152	37.80	12.307
x_1x_3	9.26	25.956	30.24	111.320

note that the index i labels the slot taken by the down quark (counting from the right), and the quark with helicity opposite to the proton's momentum is always in the middle slot. There is only one independent distribution amplitude, ϕ_1, the others being related to it by

$$\begin{aligned}\phi_2(x_1,x_2,x_3) &= -[\phi_1(x_1,x_2,x_3)+\phi_1(x_3,x_2,x_1)],\\ \phi_3(x_1,x_2,x_3) &= \phi_1(x_3,x_2,x_1).\end{aligned} \tag{3.8}$$

The state with $h=-1$ is obtained by flipping the helicity of all the quarks in Eq. (3.7); neutron states are obtained by switching up and down quarks and multiplying the state by -1.

The distribution amplitude is weakly dependent on renormalization scale Q:

$$\phi(x_1,x_2,x_3) = 120x_1x_2x_3\sum_n a_n(Q^2)\tilde{\phi}_n(x_1,x_2,x_3), \tag{3.9}$$

where the $\tilde{\phi}_n(x_1,x_2,x_3)$ are the Appell polynomials, which are orthonormal on the measure $120x_1x_2x_3[dx]$. The expansion coefficients, or moments, are matrix elements of three-quark operators, renormalized at $\mu^2=Q^2$: $f_N a_n(Q^2) = \langle 0|O_n|p_\uparrow\rangle$. The Q^2 dependence is due to anomalous dimensions of the O_n. There are theoretical calculations of the first six a_n at $Q^2\approx 1$–2 GeV^2, using QCD sum rules, which, together with other phenomenological considerations, have motivated models for the distribution amplitude. The first six moments evolve too slowly in Q^2 to affect the comparison with experiment, so we have neglected the evolution. Instead we have used four different model distribution amplitudes [11, 12, 13, 14] to investigate the impact of the distribution amplitude on the results. The asymptotic distribution function $\phi_{as}(x) = 120x_1x_2x_3$ is as apt at present energies as the asymptotic δ-function structure function.

The first six moments only involve Appell polynomials of degree no higher than quadratic. Table 1 gives the coefficients of the listed monomials for ϕ_1, after eliminating $x_2 = 1-x_1-x_3$ entirely. The coefficients for ϕ_2 can be obtained from Table 1 and Eq. (3.8). The numbers may appear unfamiliar to experts, because Eqs. (3.6), (3.7) and (3.8) are cast in a way convenient for convoluting the distribution amplitude with the hard-scattering amplitude, rather than the arrangement used in the sum-rule analyses.

3.2 Hard-scattering amplitude

There are 378 Feynman diagrams contributing to the hard-scattering amplitude. They can be classified according to the arrangement of the gluon lines into seven groups, as illustrated in Fig. 3.

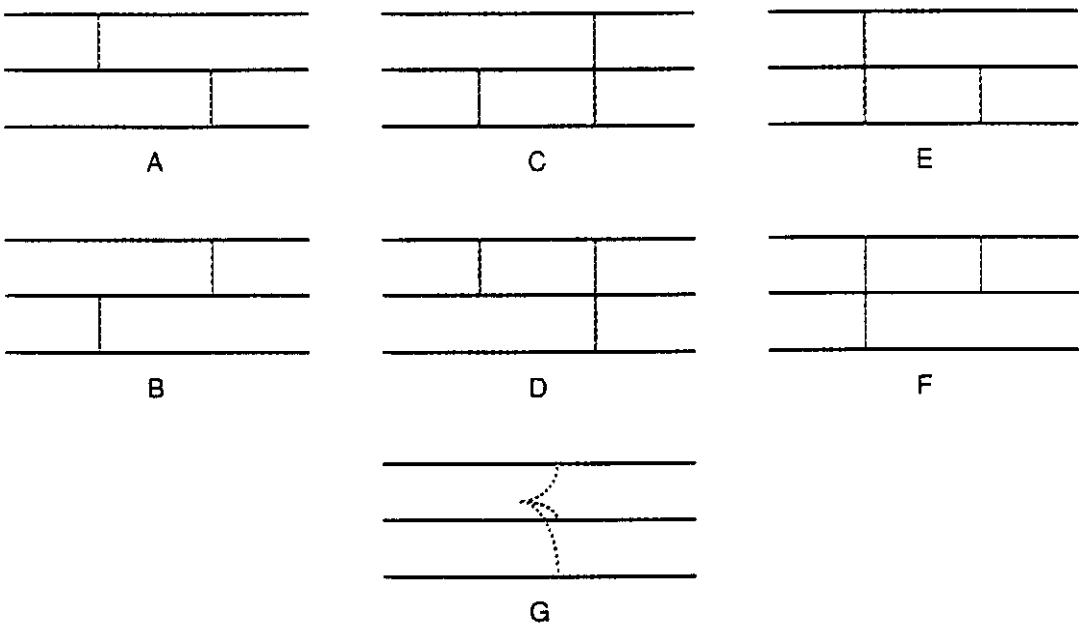

Figure 3: The seven ways of arranging gluon lines in the Feynman diagrams.

In Group G there are 42 ways of attaching the two photons, but the color factor vanishes. In Groups A–F there are 56 ways of attaching the two photons, and the color factor is $[(N+1)/2N]^2$ ($= 4/9$ for $N = 3$). Diagrams in Groups B, D and F may be obtained from A, C and E, respectively, by

$$\mathcal{E}: \; x_1 \leftrightarrow x_3, \; y_1 \leftrightarrow y_3, \text{ and } e_1 \leftrightarrow e_3. \tag{3.10}$$

The calculation of the hard-scattering amplitude is easiest using the helicity formalism outlined in Ref. [2]. We have used this formalism to compute all diagrams in Groups A, C and E for $h = h' = +1$. We found it convenient to assign arbitrary helicity to the (on-shell) photons,

$$\begin{aligned} |\gamma_{\text{in}}\rangle &= \alpha|\uparrow\rangle + \beta|\downarrow\rangle, \\ |\gamma_{\text{out}}\rangle &= \gamma|\uparrow\rangle + \delta|\downarrow\rangle. \end{aligned} \tag{3.11}$$

This approach provides all four amplitudes with photon helicities λ, $\lambda' = \pm 1$, which is redundant, cf. Eq. (3.5), but useful. Table 2 shows the number of diagrams in these groups that vanish (for massless quarks) and that have one, two or three propagators that can go on shell. We sort the diagrams according to the number of potentially on-shell propagators, and we tailor the integration over momentum fractions to each case separately.

By time reversal symmetry each diagram in Groups A, C and D is related to one in Groups B, E and F by

$$\mathcal{T}: \; \alpha \leftrightarrow \gamma, \; \beta \leftrightarrow \delta, \text{ and } x_i \leftrightarrow y_i, \; \forall i. \tag{3.12}$$

We have used the operation $\mathcal{T}$ to check Group C vs. Group E and the composition $\mathcal{T} \circ \mathcal{E}$ to check Group A vs. itself. (The check on Group A almost always relates distinct diagrams, so it is not trivial.) These checks were easy to carry out efficiently, because we had used the photon states in Eq. (3.11).

Appendix B tabulates the contributions $\bar{T}^{(d)}(x, h, \lambda; y, h', \lambda')$ of all non-zero diagrams, in a way that makes clear the relations implied by the operation $\mathcal{E}$, $\mathcal{T}$ and $\mathcal{T} \circ \mathcal{E}$.

Table 2: Number of diagrams that vanish or have one, two or three propagators that can go on shell.

Group	vanish	no props.	one prop.	two props.	three props.
A	12	8	12	16	8
C	30	6	8	8	4
E	30	6	8	8	4

3.3 Convolution of hard-scattering amplitude with distribution amplitude

In addition to using the operations $\mathcal{E}$ and $\mathcal{T}$ to check the calculations, one can also use them to simplify the convolution. One can restrict the sum to diagrams $d \in A \cup C \cup E$ in the following way. Consider the sum of the contributions from diagrams d and $\mathcal{E}(d)$. Using Eq. (3.10), relabeling the integration variables and exploiting $Z_i^{(\mathcal{E}(d))} = Z_{\mathcal{E}(i)}^{(d)}$, $\phi_i(\mathcal{E}(x)) = \phi_{\mathcal{E}(i)}(x)$, yields

$$\mathcal{M} = 2\frac{4}{9}g^4 \sum_{d\in A\cup C\cup E} \int [dx][dy]\, \tilde{T}^{(d)}(x;y) \sum_i \left(Z_i^{(d)} \phi_i(x) \phi_i^*(y) \right), \tag{3.13}$$

where nonessential labels have been suppressed. Similarly, when $\lambda = \lambda'$ one can relate the contributions from diagrams d and $\mathcal{T}(d)$ and reduce the range of the sum further, in favor of another factor of 2.

We have tried to integrate analytically over as many of the momentum fractions as we can. In an automated computer approach, these integrals could be done symbolically. The basic strategy starts with eliminating one each of the x and y momentum fractions, and rescaling another so that the integration region is a unit square. For example,

$$\int [dx] F(x_1, x_2, x_3) = \int_0^1 dx_1 \int_0^{\bar{x}_1} dx_3 \tilde{F}(x_1, x_3) = \int_0^1 dx_1 \int_0^1 dx_3 \bar{x}_1 \tilde{F}(x_1, \bar{x}_1 x_3), \tag{3.14}$$

where $\tilde{F}(x_1, x_3) = F(x_1, 1-x_1-x_3, x_3)$ and $\bar{x}_i = 1 - x_i$. (We do not necessarily eliminate x_2; when x_2 appears in the propagator of a line that can go on shell, we then use Eq. (3.14) to eliminate x_1 or x_3.) Naturally, the difficulty of performing the integral increases as more internal lines can go on shell. We discuss the various cases separately:

3.3.1 No propagators on shell

Here all momentum-fraction integrals decouple, leaving products of

$$\int dx x^{m-1} \bar{x}^{n-1} = B(m,n) = \frac{\Gamma(m)\,\Gamma(n)}{\Gamma(m+n)}. \tag{3.15}$$

All these diagrams can be integrated analytically/symbolically.

3.3.2 One propagator on shell

Here the momentum-fraction integrals for the initial and final states are coupled by a denominator of the form

$$\frac{1}{\xi(1-\eta s^2) - \eta c^2 + i\varepsilon} = \mathrm{P}\frac{1}{\xi(1-\eta s^2) - \eta c^2} - i\pi\delta(\xi(1-\eta s^2) - \eta c^2), \tag{3.16}$$

where $\xi \in \{x_1, x_2, x_3, \bar{x}_1, \bar{x}_2, \bar{x}_3\}$, $\eta \in \{y_1, y_2, y_3, \bar{y}_1, \bar{y}_2, \bar{y}_3\}$ and "P" stands for principal part. The numerator is a polynomial in ξ and η, and the momentum fractions other than ξ and η. For the imaginary part, the integral over ξ, say, is carried out using the δ-function in Eq. (3.16), and the η integral is carried out analytically. For the real part, the integral over ξ is carried out analytically, leaving a mundane, if complicated, integral over η, which is carried out numerically. In both cases the momentum fractions other than ξ and η can be carried out using Eqs. (3.14) and (3.15).

3.3.3 Two propagators on shell

Here there are two denominators of the form in Eq. (3.16), but the domain of integration with both lines on shell is of measure zero. For details see Appendix C, which presents the evaluation of a diagram from this class in detail.

For the two contributions to the imaginary part, the momentum-fraction integrals can be reduced to the hypergeometric function. The imaginary part from this class of diagrams makes the largest contribution to the scattering amplitude, and we have evaluated it with no numerical uncertainty (except round-off).

For the real part, we perform numerically a two dimensional integral of the form

$$\int_0^1 d\eta \int_0^1 d\xi\, \Omega(\xi,\eta)\, \mathrm{P} \frac{1}{\xi(1-\eta s^2) - \eta c^2}, \tag{3.17}$$

where $\Omega(\xi,\eta)$ is the result of performing the other principal part integral analytically. It is important to treat Eq. (3.17) in a numerically robust way. We have used the method of Ref. [4], which ensures that the large peaks on either side of the pole cancel point-by-point. Appendix D reviews this method, and compares it to the method of Ref. [9], of keeping ε small but finite.

3.3.4 Three propagators on shell

Here there are three denominators of the form in Eq. (3.16): two gluon lines and a quark line. The kinematics permit both gluons to be on shell simultaneously, but if the quark is on shell, the gluons must be off shell, except on a set of measure zero.

For the imaginary part, there are three contributions, each of which can be reduced to two-dimensional integrals. One integration is trivial, using the δ-function of Eq. (3.16). It is possible to perform another integral analytically, even when the δ-function comes from a gluon line, in which case, the integral over the momentum fractions in the other gluon line is defined by the principal part.

The real part has two distinct contributions: when no line is on shell, or when both gluons are on shell. In both cases, the principal part of the momentum fractions in the quark line is treated using the method in Appendix D. The other momentum fractions are handled analytically, using either Eq. (3.14), the hypergeometric function, or δ-functions.

4 Results and Discussion

The spin-polarized cross section is given by

$$\frac{d\sigma^{\lambda\lambda'}_{h h'}(s,t)}{dt} = \frac{1}{16\pi s^2} |\mathcal{M}^{\lambda\lambda'}_{h h'}(s,t)|^2. \tag{4.1}$$

Our results for $s^6 d\sigma/dt$ are plotted in Fig. 4 for the proton and in Fig. 5 for the neutron. We present the three polarization combinations in Eq. (3.5), as well as the unpolarized cross section

$$\frac{d\sigma(s,t)}{dt} = \frac{1}{4} \sum_{h,h',\lambda,\lambda'} \frac{d\sigma_{hh'}^{\lambda\lambda'}(s,t)}{dt}. \tag{4.2}$$

We evaluated the helicity amplitudes in steps of 10° for $20° \leq \theta \leq 160°$ and interpolated the real and imaginary parts *separately*, using cubic splines. Four different distribution amplitudes are shown, CZ (dashed lines) [11], COZ (solid lines) [12], KS (dotted lines) [13], GS (dot-dashed lines) [14]. Fig. 4(d) also includes the data from the Tufts-MIT-Cornell experiment [5]. Perturbative QCD (with assistance from QCD sum rules) agrees well with the data, especially in light of uncertainties in the normalization, discussed below.

Figs. 6 and 7 exhibit our results for the phase of the amplitude, as a function of center-of-mass scattering angle. Since the real and imaginary parts are both $O(\alpha_S)$, the phases are $O(1)$.

There are a few features of the plots that, perhaps, should be pointed out. In general, the real and imaginary parts of the amplitudes vanish at some value of θ, in which case the phase is a multiple of 90°. Sometimes these zeros appear at nearly the same θ, leading to deep dips in the cross section. The GS distribution amplitude, which incorporates assumptions about nucleon structure, gives results that are frequently quite distinct from the others. Finally, the neutron, which interacts electromagnetically only because of its sub-structure, has a Compton cross section about the same size as that of the proton.

According to the dimensional counting rules [18, 1], $s^6 d\sigma/dt$ should be independent of s. In QCD, several effects lead to deviations from this rule. First, there is the running of the QCD coupling constant, which we have fixed at $\alpha_S = 0.3$, as in the previous perturbative-QCD calculations [15, 9]. Our leading order calculation of the cross section is sensitive to this choice, because it is proportional to α_S^4, but the dependence is purely multiplicative. Second, there is the running of the distribution amplitude, which enters in a very complicated way. The dependence of our predictions on the distribution amplitude gives a qualitative estimate of this effect: it is of the same magnitude as the experimental data's violation of the dimensional counting rules. Third, there are mass effects, because the calculation was done neglecting quark (and nucleon) masses, but the laboratory energies E_γ of photon beams in the experiment [5] are not high enough to neglect the proton mass in determining $s = 2E_\gamma m_p + m_p^2$. Finally, there are higher twist effects, coming from scattering of non-valence Fock states in the proton or photon. The most important of these is the $q\bar{q}$ component of the photon, whose contribution to the amplitude is suppressed by only one power of s [1].

The largest systematic uncertainty in our predictions comes from the nucleon decay constant. The cross section is proportional to f_N^4, and we have used the value $f_N = (5.2 \pm 0.3) \times 10^{-3}$ GeV^2 suggested by QCD sum rules [11, 13]. Accepting the error estimate at face value yields a 23% uncertainty in the cross sections. On the other hand, using the value suggested by quenched lattice QCD [10], $f_N = (2.9 \pm 0.6) \times 10^{-3}$ GeV^2, would reduce the cross section by a factor of 9. (Such a substitution is a bit simple-minded; it would be more sensible to compute several moments in lattice QCD and use a distribution amplitude derived from those moments.) The lack of agreement between theoretical calculations of the decay constant underscore the need to determine it directly from the data.

Two previous papers [15, 9] have attempted the calculations presented here and have obtained different results. Unfortunately, we do not verify either one. For the CZ distribution amplitude our results for the cross section are smaller than those of Ref. [15] and larger than Ref. [9]. Furthermore, as a function of θ the phases in refs. [15, 9] do not resemble ours at all. For $\theta > 90°$ the discrepancy

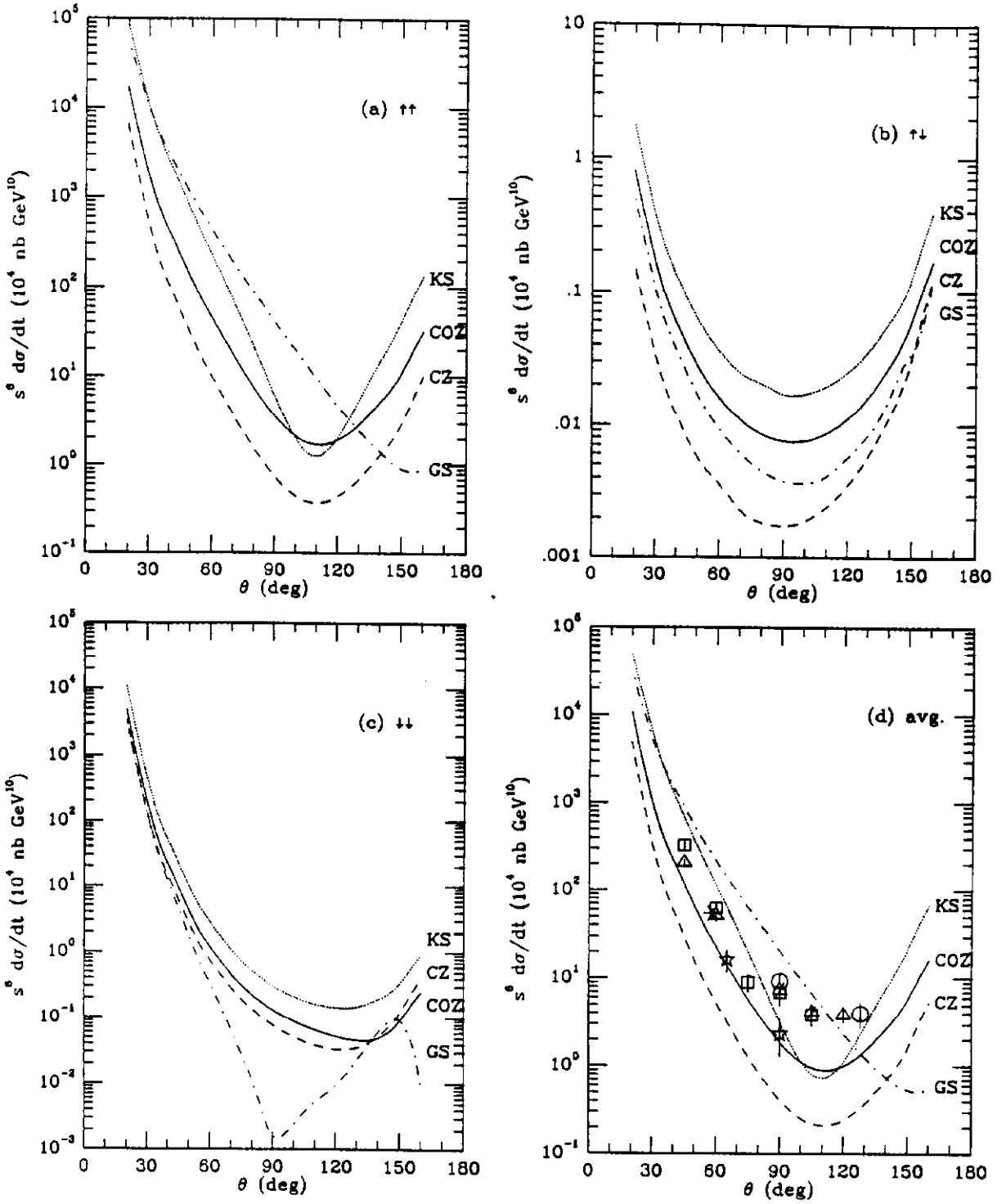

Figure 4: Differential cross sections for (a) $\gamma_\uparrow p_\uparrow \to \gamma_\uparrow p_\uparrow$, (b) $\gamma_\uparrow p_\uparrow \to \gamma_\downarrow p_\uparrow$, (c) $\gamma_\downarrow p_\uparrow \to \gamma_\downarrow p_\uparrow$, and (d) unpolarized proton Compton scattering. The experimental data [5] in (d) are at s = 4.63 GeV (circles), s = 6.51 GeV (triangles), s = 8.38 GeV (squares), s = 10.26 GeV (five-pointed stars), and s = 12.16 GeV (asterisk).

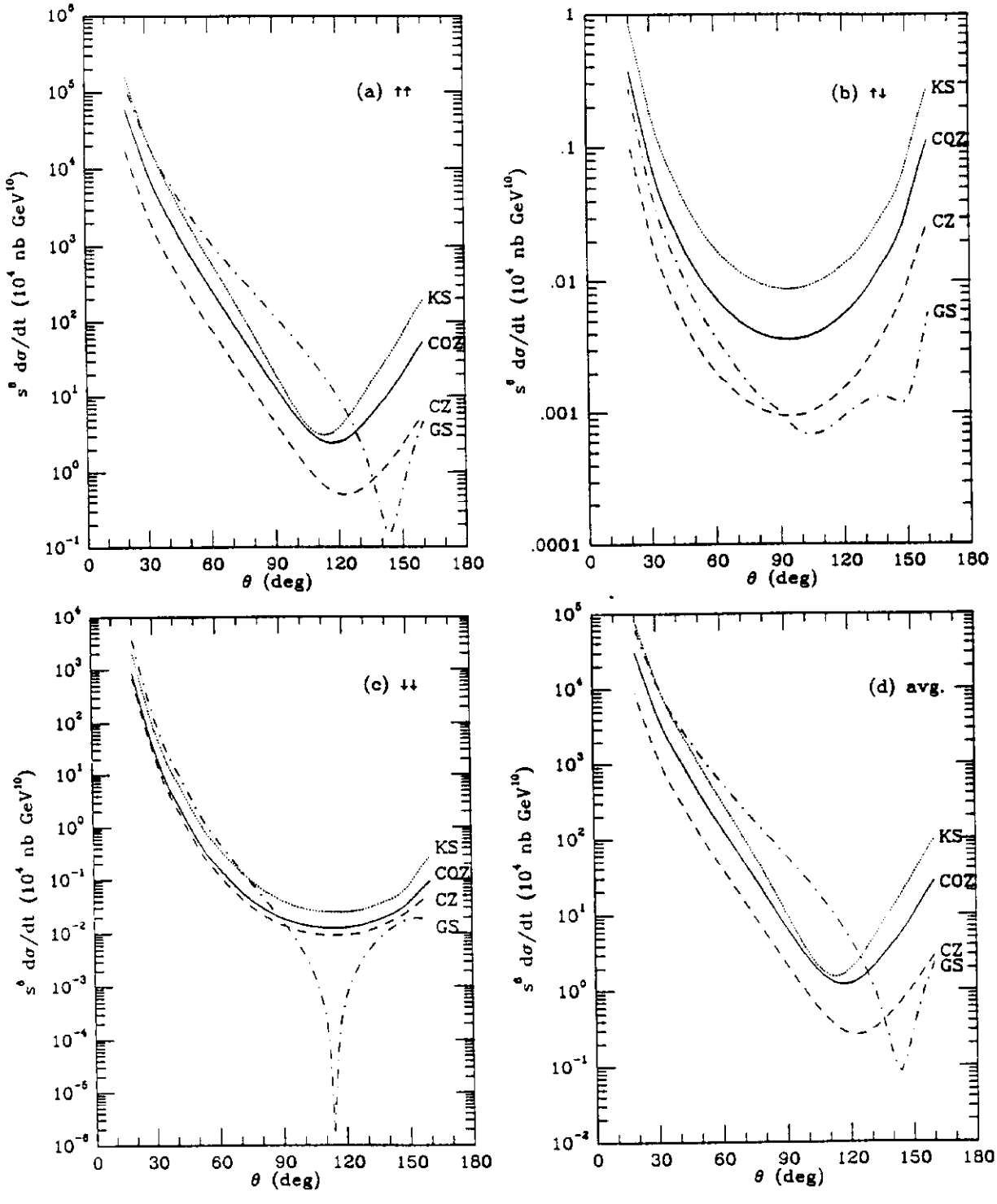

Figure 5: Differential cross sections for (a) $\gamma_\uparrow n_\uparrow \to \gamma_\uparrow n_\uparrow$, (b) $\gamma_\uparrow n_\uparrow \to \gamma_\downarrow n_\uparrow$, (c) $\gamma_\downarrow n_\uparrow \to \gamma_\downarrow n_\uparrow$, and (d) unpolarized neutron Compton scattering.

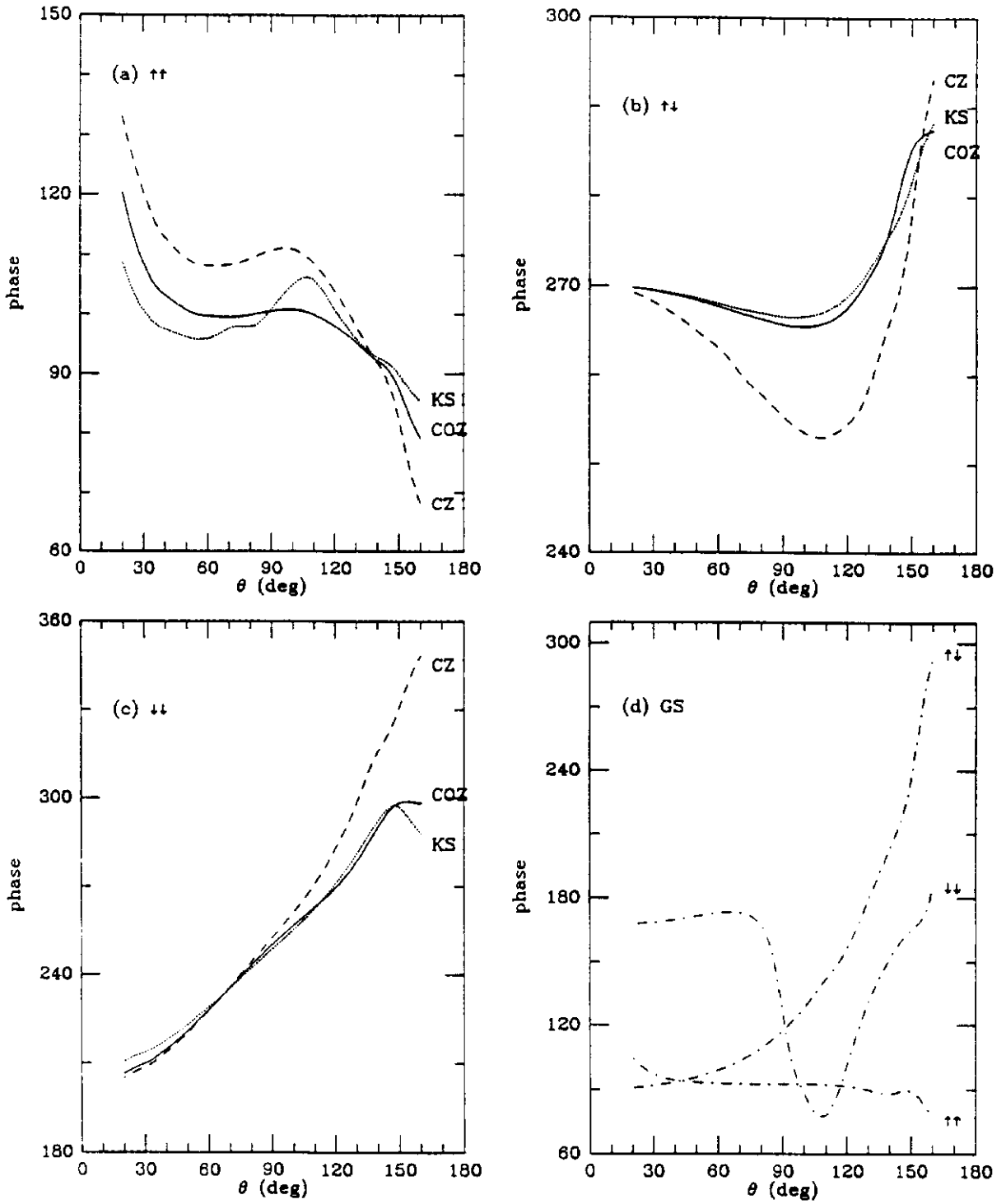

Figure 6: Phase of the amplitude for (a) $\gamma_\uparrow p_\uparrow \to \gamma_\uparrow p_\uparrow$, (b) $\gamma_\uparrow p_\uparrow \to \gamma_\downarrow p_\uparrow$, (c) $\gamma_\downarrow p_\uparrow \to \gamma_\downarrow p_\uparrow$, and (d) all helicity combinations for the Gari-Stefanis distribution amplitude [14].

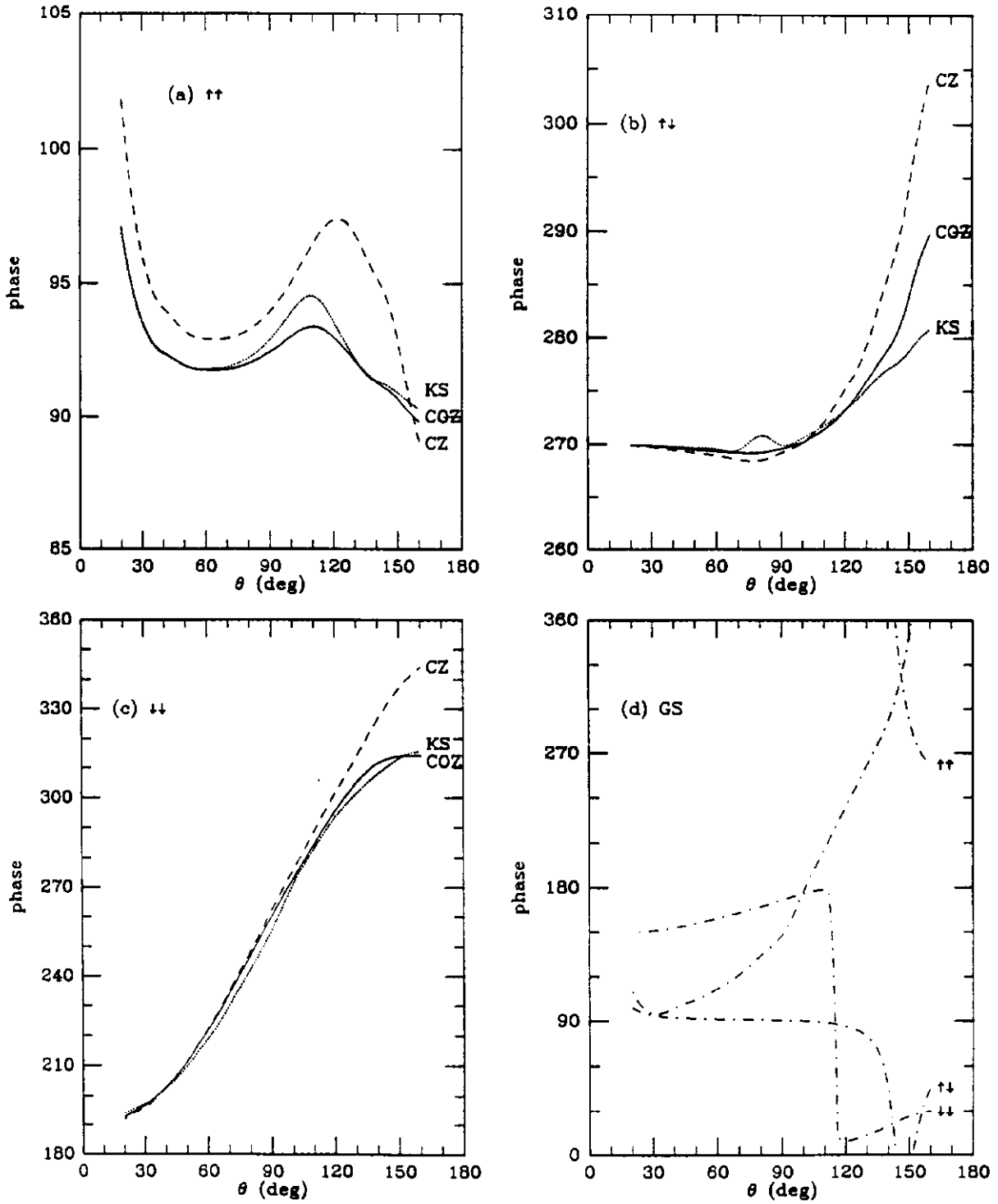

Figure 7: Phase of the amplitude for (a) $\gamma_\uparrow n_\uparrow \to \gamma_\uparrow n_\uparrow$, (b) $\gamma_\uparrow n_\uparrow \to \gamma_\downarrow n_\uparrow$, (c) $\gamma_\downarrow n_\uparrow \to \gamma_\downarrow n_\uparrow$, and (d) all helicity combinations for the Gari-Stefanis distribution amplitude [14].

in the cross section is as large as a factor of five. In our opinion, it arises from those references' treatment of the on-shell parton lines. Reference [9] maintains that the method of Ref. [15] is incorrect. However, our tests of Ref. [9]'s $i\varepsilon$-method did not succeed in evaluating correctly the imaginary part of diagrams where two internal lines can go on shell, which typically makes the largest contribution to the amplitude. The $i\varepsilon$-method replaces the on-shell δ-function by a sharp Lorentzian peak. Consequently, the four-dimensional integral comes from the neighborhood of a three-dimensional hypersurface. This hypersurface is not aligned with any of the integration axes, making it exceedingly difficult to integrate numerically. It is much better to integrate a δ-function the old-fashioned way—by hand.

5 Conclusions

This paper has presented our results for wide-angle nucleon Compton scattering in leading-order perturbative QCD. This is a challenging calculation for two reasons. First, there are 52 independent, non-zero diagrams contributing to the scattering amplitude. We have been very careful to evaluate them this correctly. Each author independently worked out all diagrams in classes A, C, and E (cf. Fig. 3), of which 72 vanish and 96 are non-zero. We then eliminated algebraic slip-ups by applying Eq. (3.12) and by comparing the two lists of results. Second, the momentum-fraction integrals are not straightforward. Internal partons can go on shell, and the associated singularities in the integrands must be treated with caution. Our approach has been to perform these integrals analytically, wherever possible, or use the robust technique outlined in Appendix D [4] and VEGAS [3].

With any leading-order perturbative calculation, the question of higher order corrections arises. While one would not expect them to alter the qualitative agreement between theory and experiment, they would assist the experimental determination of the distribution amplitude. Without higher order corrections it is impossible to extract the nucleon decay constant reliably. The cross section is proportional to $(\alpha_S f_N)^4$, and the higher-order corrections are needed to pin down the ambiguity in the running of the coupling constant. Deviations from the energy dependence suggested by dimensional counting rules may prove useful in determining the higher moments. Finally, it is plausible that higher-order QCD will better describe the flatness in the angular distribution for $\theta > 75°$. Of course, calculating the higher order corrections will be impossible without carefully designed computer programs to generate and evaluate the diagrams quickly and to perform the loop and momentum-fraction integrals correctly.

To assess the experimental prospects one must appreciate the steep s^{-6} fall-off of the cross section. Let us use the experimental cross section [5] and this rule, and, for the sake of argument, let us suppose measurements of the differential cross section $d\sigma/d(\cos\theta)$ are possible at the level of picobarns. In a colliding beam experiment, set up so that the incident photon and proton have equal energy, one has $dt = s\, d(\cos\theta_{\rm c.m.})$, and experiments are feasible for $s < 40$–60 GeV^2. In a fixed target experiment, unless $\theta_{\rm lab} \ll 1$ one has $dt \propto m_N^2\, d(\cos\theta_{\rm lab})$, and experiments are feasible for $s < 20$–30 GeV^2.

At HERA the kinematics are more involved, because of the high electron-proton center-of-mass energy, and because of the asymmetry in the energies of the beams. For example, the incident photon is virtual with $k^2 = -Q^2$ negative. When $Q^2 \lesssim s_{\gamma p} \approx 40$–$60$ GeV^2, the case for which we have results, the outgoing photon and proton are very energetic, but emerge nearly parallel to the proton beam. When $Q^2 \gg s_{\gamma p}$ the outgoing particles emerge at wide angles, but their energies are low. At best, then, there might be an intermediate region, where the final state is easy to detect, yet $s_{\gamma p}$ is neither too small nor too large.

Reference [9] presented results for nucleon Compton scattering when $Q^2 \neq 0$, as well as $\gamma B \to \gamma B'$, where B (B') is a nucleon or a Δ resonance. More recently, results have appeared for the family of processes $\gamma p \to MB$, where M is a meson and B a baryon [19]. The on-shell propagators were treated by the $i\epsilon$-method. We hope that these processes will be re-evaluated using our analytical and numerical techniques. The details in the appendices and sec. 3 should prove helpful in this undertaking.

Large momentum-transfer exclusive processes are important because they test QCD in a way complementary to inclusive reactions. For example, the distribution amplitude is proportional to the hadron wave function, whereas the structure functions are proportional to the square. Data exist for several γp processes as well as $\gamma\gamma \to p\bar{p}$. With an appropriate battery of analytical and numerical techniques, it may be possible to extract the nucleon distribution amplitude from experiment. The moments of $\phi(x_1, x_2, x_3)$ could then be compared directly to theory, as non-perturbative QCD calculations improve. This approach is probably sounder than the present strategy—taken in this paper and elsewhere—of using model distribution amplitudes that unrealistically neglect higher moments.

Acknowledgements

We would like to thank G.P. Lepage for useful discussions. Part of this paper was written while A.S.K. was visiting the Institute for Theoretical Physics in Santa Barbara, which is supported by the National Science Foundation under Grant No. PHY89-04035.

A Kinematics and Spinor Algebra

This appendix collects our conventions for the kinematics and spinor algebra used to compute the Compton scattering cross sections.

A.1 External momenta

Let p and k (p' and k') be the incoming (outgoing) nucleon and photon momenta, respectively. In the center-of-mass frame these vectors have Cartesian components

$$\begin{aligned} p &= E(1,0,0,1), \\ k &= E(1,0,0,-1), \\ p' &= E(1,\sin\theta,0,\cos\theta), \\ k' &= E(1,-\sin\theta,0,-\cos\theta), \end{aligned} \tag{A.1}$$

where θ is the scattering angle and the azimuthal angle has been set to zero. It is more convenient to work with light-cone components, defined for arbitrary vector v by

$$\begin{aligned} v^+ &= \tfrac{1}{\sqrt{2}}(v^0 + v^3), \quad v^- = \tfrac{1}{\sqrt{2}}(v^0 - v^3), \\ v^L &= \tfrac{1}{\sqrt{2}}(v^1 + iv^2), \quad v^R = \tfrac{1}{\sqrt{2}}(v^1 - iv^2). \end{aligned} \tag{A.2}$$

The dot product of two vectors is then $v \cdot w = v^+w^- + v^-w^+ - v^Lw^R - v^Rw^L$. In light-cone components $(+,-,L,R)$ Eq. (A.1) can be re-written:

$$\begin{aligned} p &= \sqrt{2}E(1,0,0,0), \\ k &= \sqrt{2}E(0,1,0,0), \\ p' &= \sqrt{2}E(c^2,s^2,sc,sc), \\ k' &= \sqrt{2}E(s^2,c^2,-sc,-sc), \end{aligned} \tag{A.3}$$

where $s = \sin(\frac{1}{2}\theta)$ and $c = \cos(\frac{1}{2}\theta)$.

The Mandelstam invariants, neglecting masses, are

$$\begin{aligned} s &= (p+k)^2 = (p'+k')^2 = 4E^2, \\ t &= (p-p')^2 = (k'-k)^2 = -4E^2s^2, \\ u &= (p-k')^2 = (p'-k)^2 = -4E^2c^2, \end{aligned} \tag{A.4}$$

with $s + t + u = 0$. These variables are useful in writing manifestly invariant expressions, using $s = \sqrt{-t/s}$ and $c = \sqrt{-u/s}$. In particular, they make easy the check of our calculations against the reaction $\gamma\gamma \to p\bar{p}$, which is related by crossing.

A.2 Photon polarization

Let the incoming (outgoing) photon polarization vector be denoted by ϵ_i (ϵ_f); the Cartesian components are

$$\begin{aligned} \epsilon_i(\uparrow) &= \tfrac{1}{\sqrt{2}}(1,-i,0), & \epsilon_i(\downarrow) &= -\tfrac{1}{\sqrt{2}}(1,i,0), \\ \epsilon_f(\uparrow) &= \tfrac{1}{\sqrt{2}}(\cos\theta,-i,-\sin\theta), & \epsilon_f(\downarrow) &= -\tfrac{1}{\sqrt{2}}(\cos\theta,i,-\sin\theta), \end{aligned} \tag{A.5}$$

following Messiah's conventions [20]. Note that k points along the negative z-axis, that k' is at angle $\pi + \theta$ to the z-axis, and that $\epsilon(\downarrow) = -\epsilon(\uparrow)^*$.

The time component of the four-vectors corresponding to all polarization vectors is 0. The light-cone components $(+,-,L,R)$ are:

$$\begin{aligned} \epsilon_i(\uparrow) &= (0,0,1,0), & \epsilon_i(\downarrow) &= (0,0,0,-1), \\ \epsilon_f(\uparrow) &= (-sc,+sc,c^2,-s^2), & \epsilon_f(\downarrow) &= (+sc,-sc,s^2,-c^2). \end{aligned} \tag{A.6}$$

The states defined in Eq. (3.11) have polarization

$$\epsilon_i = \alpha\epsilon_i(\uparrow) + \beta\epsilon_i(\downarrow) \quad \text{and} \quad \epsilon_f = \gamma\epsilon_f(\uparrow) + \delta\epsilon_f(\downarrow). \tag{A.7}$$

A.3 Dirac matrices

We use the chiral representation of the Dirac matrices, i.e. γ_5 is diagonal:

$$\gamma_5 = \gamma^5 = i\gamma^0\gamma^1\gamma^2\gamma^3 = \begin{pmatrix} 1 & 0 \\ 0 & -1 \end{pmatrix}. \tag{A.8}$$

The matrices γ^μ and $\not{q}$ are given by

$$\gamma^\mu = \begin{pmatrix} 0 & \gamma^\mu_+ \\ \gamma^\mu_- & 0 \end{pmatrix}, \quad \not{q} = \begin{pmatrix} 0 & \not{q}_+ \\ \not{q}_- & 0 \end{pmatrix}, \tag{A.9}$$

where $\gamma^\mu_\pm = (-1, \pm\boldsymbol{\sigma})$.

Momenta of fermion lines are represented by two-by-two matrices $\not{q}_\pm = -(q^0 1 \pm \boldsymbol{q}\cdot\boldsymbol{\sigma})$ in the helicity formalism. The subscript is chosen according to the helicity of the fermion line in question. Explicitly,

$$\not{q}_+ = -\sqrt{2}\begin{pmatrix} q^+ & q^R \\ q^L & q^- \end{pmatrix}, \quad \not{q}_- = -\sqrt{2}\begin{pmatrix} q^- & -q^R \\ -q^L & q^+ \end{pmatrix}. \tag{A.10}$$

In particular, the external momenta take form:

$$\not{p}_+ = \not{k}_- = -2E\begin{pmatrix} 1 & 0 \\ 0 & 0 \end{pmatrix}, \quad \not{p}_- = \not{k}_+ = -2E\begin{pmatrix} 0 & 0 \\ 0 & 1 \end{pmatrix}, \tag{A.11}$$

and

$$\not{p}'_+ = \not{k}'_- = -2E\begin{pmatrix} c^2 & sc \\ sc & s^2 \end{pmatrix}, \quad \not{p}'_- = \not{k}'_+ = -2E\begin{pmatrix} s^2 & -sc \\ -sc & c^2 \end{pmatrix}; \tag{A.12}$$

and the polarization vectors take the form

$$\not{\epsilon}_{i+} = \sqrt{2}\begin{pmatrix} 0 & \beta \\ -\alpha & 0 \end{pmatrix} = -\not{\epsilon}_{i-}, \quad \not{\epsilon}^*_{f+} = \sqrt{2}\begin{pmatrix} (\gamma-\delta)sc & -\gamma c^2 - \delta s^2 \\ \gamma s^2 + \delta c^2 & (\delta-\gamma)sc \end{pmatrix} = -\not{\epsilon}^*_{f-}. \tag{A.13}$$

A.4 Quark wave functions

In computing the hard-scattering amplitude, the appropriate factors for the external quark lines are $u_\pm(xp)/\sqrt{x} = u_\pm(p)$. These are

$$u_+(p) = \sqrt{2E}\begin{pmatrix} 1 \\ 0 \end{pmatrix}, \quad u_-(p) = \sqrt{2E}\begin{pmatrix} 0 \\ 1 \end{pmatrix} \tag{A.14}$$

for incoming quarks and

$$u_+(p') = \sqrt{2E}\begin{pmatrix} c \\ s \end{pmatrix}, \quad u_-(p') = \sqrt{2E}\begin{pmatrix} -s \\ c \end{pmatrix} \tag{A.15}$$

for outgoing quarks, where the subscript denotes the helicity. As explained in Ref. [2] one occasionally charge conjugates a quark line; in the Compton scattering calculation, this must be done for diagrams in Groups C and E. The charge-conjugate wave functions are:

$$\tilde{u}_-(p) = i\sigma_2 u^*_+(p) = \sqrt{2E}\begin{pmatrix} 0 \\ -1 \end{pmatrix}, \quad \tilde{u}_-(p') = i\sigma_2 u^*_+(p') = \sqrt{2E}\begin{pmatrix} s \\ -c \end{pmatrix}. \tag{A.16}$$

Table 3: Non-zero contributions to $\tilde{T}^{(d)}(x,\uparrow,\lambda;y,\uparrow,\lambda')$ from Group A, and hence Group B, which is obtained using the operations $\mathcal{E}$ and $\mathcal{T}$. The operation $\mathcal{T}\circ\mathcal{E}$ usually generates a distinct diagram, so we do not list both expressions. When $\mathcal{T}\circ\mathcal{E}$ returns the same diagram, we enclose the diagram label in parentheses, to emphasize that it should not be counted twice.

d $\mathcal{E}(d)$	$\mathcal{T}(d)$ $\mathcal{T}\circ\mathcal{E}(d)$	$\tilde{T}^{(d)}(x,\uparrow,\uparrow;y,\uparrow,\uparrow)$	$\tilde{T}^{(d)}(x,\uparrow,\uparrow;y,\uparrow,\downarrow)$	$\tilde{T}^{(d)}(x,\uparrow,\downarrow;y,\uparrow,\uparrow)$	$\tilde{T}^{(d)}(x,\uparrow,\downarrow;y,\uparrow,\downarrow)$
$A11$ $B66$	$B22$ $A77$	$\dfrac{-c}{s^4}\dfrac{1}{x_1\bar{x}_1^2x_3\bar{y}_1^2y_3}$	0	0	0
$\overline{A11}$ $\overline{B66}$	$\overline{B22}$ $\overline{A77}$	$\dfrac{-1}{s^2c}\dfrac{1}{\bar{x}_1^2x_3\bar{y}_1^2y_3}$	$\dfrac{-1}{s^2c}\dfrac{1}{x_1\bar{x}_1x_3\bar{y}_1^2y_3}$	0	$\dfrac{-c}{s^4}\dfrac{1}{x_1\bar{x}_1^2x_3\bar{y}_1^2y_3}$
$A12$ $B67$	$B12$ $A67$	$\dfrac{c}{s^4}\dfrac{1}{x_1\bar{x}_1x_3y_1\bar{y}_1^2y_3}$	0	0	0
$A21$ $B76$	$B21$ $A76$	0	$\dfrac{1}{s^2c}\dfrac{1}{x_1\bar{x}_1x_3\bar{y}_1^2y_3}$	0	$\dfrac{1}{s^4c}\dfrac{1-y_1s^2}{x_1\bar{x}_1x_3y_1\bar{y}_1^2y_3}$
$A13$ $B63$	$B52$ $A57$	$\dfrac{1}{s^2c}\dfrac{1-x_2s^2}{x_1x_2x_3\bar{y}_1y_3(x_1,y_1)}$	$\dfrac{1}{c}\dfrac{1}{x_1x_3\bar{y}_1y_3(x_1,y_1)}$	0	0
$A31$ $B36$	$B25$ $A75$	0	0	0	$\dfrac{c}{s^2}\dfrac{1}{x_1x_2x_3\bar{y}_1y_3(y_1,x_1)}$
$A14$ $B64$	$B42$ $A47$	$-c\dfrac{x_3-\bar{y}_1}{x_1x_3\bar{y}_1y_3(x_1,y_1)(\bar{x}_3,y_1)}$	$-c\dfrac{\bar{x}_3}{x_1x_3\bar{y}_1y_3(x_1,y_1)(\bar{x}_3,y_1)}$	0	0
$A41$ $B46$	$B24$ $A74$	$-\dfrac{1}{c}\dfrac{1-\bar{y}_1s^2}{x_3\bar{y}_1y_3(y_1,x_1)(y_1,\bar{x}_3)}$	$-\dfrac{1}{c}\dfrac{1}{x_1x_3\bar{y}_1y_3(y_1,\bar{x}_3)}$	0	0

Table 3: (cont.)

d / $\mathcal{E}(d)$	$\mathcal{T}(d)$ / $\mathcal{T}\circ\mathcal{E}(d)$	$\tilde{T}^{(d)}(x,\uparrow,\uparrow;y,\uparrow,\uparrow)$	$\tilde{T}^{(d)}(x,\uparrow,\uparrow;y,\uparrow,\downarrow)$	$\tilde{T}^{(d)}(x,\uparrow,\downarrow;y,\uparrow,\uparrow)$	$\tilde{T}^{(d)}(x,\uparrow,\downarrow;y,\uparrow,\downarrow)$
$A15$	$B32$	0	$c\dfrac{\bar{x}_3}{x_1x_3y_2y_3(x_1,y_1)(\bar{x}_3,y_1)}$	0	0
$B65$	$A37$				
$A51$	$B23$	$\dfrac{1}{c}\dfrac{1-y_2s^2}{x_3y_2y_3(y_1,x_1)(y_1,\bar{x}_3)}$	$\dfrac{1}{c}\dfrac{x_2(1-y_2s^2)}{x_1x_3y_2y_3(y_1,x_1)(y_1,\bar{x}_3)}$	$\dfrac{s^2}{c}\dfrac{1}{x_3y_3(y_1,x_1)(y_1,\bar{x}_3)}$	$\dfrac{s^2}{c}\dfrac{x_2}{x_1x_3y_3(y_1,x_1)(y_1,\bar{x}_3)}$
$B56$	$A73$				
$A16$	$B72$	$\dfrac{s^4}{c}\dfrac{\bar{x}_3}{x_1(x_1,y_1)(\bar{x}_3,y_1)(y_3,x_3)}$	$\dfrac{s^2}{c}\dfrac{\bar{x}_3(1-x_3s^2)}{x_1x_3(x_1,y_1)(\bar{x}_3,y_1)(y_3,x_3)}$	0	0
$B61$	$A27$				
$A61$	$B27$	$s^2c\dfrac{1}{x_3(y_1,x_1)(y_1,\bar{x}_3)(x_3,y_3)}$	$s^2c\dfrac{x_2}{x_1x_3(y_1,x_1)(y_1,\bar{x}_3)(x_3,y_3)}$	0	0
$B16$	$A72$				
$A17$	$(B62)$	$s^2c\dfrac{\bar{x}_3-y_1}{x_1y_3(x_1,y_1)(\bar{x}_3,y_1)(y_3,x_3)}$	0	0	0
$B62$	$(A17)$				
$A71$	$(B26)$	$\dfrac{s^4}{c}\dfrac{1}{(y_1,x_1)(y_1,\bar{x}_3)(x_3,y_3)}$	$\dfrac{s^4}{c}\dfrac{x_2}{x_1(y_1,x_1)(y_1,\bar{x}_3)(x_3,y_3)}$	$\dfrac{s^4}{c}\dfrac{y_3}{y_3(y_1,x_1)(y_1,\bar{x}_3)(x_3,y_3)}$	$\dfrac{s^2}{c}\dfrac{\bar{x}_3-y_1+s^2(\bar{x}_1\bar{y}_3+x_1y_1+x_3y_3}{x_1y_3(y_1,x_1)(y_1,\bar{x}_3)(x_3,y_3)}$
$B26$	$(A71)$				
$A24$	$B41$	$\dfrac{s^2}{c}\dfrac{1}{x_3y_3(x_1,y_1)(\bar{x}_3,y_1)}$	$c\dfrac{1}{x_3\bar{y}_1y_3(x_1,y_1)(\bar{x}_3,y_1)}$	$\dfrac{1}{c}\dfrac{1-y_1s^2}{x_3y_1y_3(x_1,y_1)(\bar{x}_3,y_1)}$	$\dfrac{c}{s^2}\dfrac{1-y_1s^2}{x_3y_1\bar{y}_1y_3(x_1,y_1)(\bar{x}_3,y_1)}$
$B74$	$A46$				
$A42$	$B14$	$\dfrac{-c}{s^2}\dfrac{1-\bar{y}_1s^2}{x_3y_1\bar{y}_1y_3(y_1,x_1)(y_1,\bar{x}_3)}$	0	0	0
$B47$	$A64$				
$A25$	$B31$	0	$-c\dfrac{1}{x_3y_2y_3(x_1,y_1)(\bar{x}_3,y_1)}$	0	$\dfrac{-c}{s^2}\dfrac{1-y_1s^2}{x_3y_1y_2y_3(x_1,y_1)(\bar{x}_3,y_1)}$
$B75$	$A36$				

Table 3: (cont.)

d $\mathcal{E}(d)$	$\mathcal{T}(d)$ $\mathcal{T}\circ\mathcal{E}(d)$	$\tilde{T}^{(d)}(x,\uparrow,\uparrow;y,\uparrow,\uparrow)$	$\tilde{T}^{(d)}(x,\uparrow,\uparrow;y,\uparrow,\downarrow)$	$\tilde{T}^{(d)}(x,\uparrow,\downarrow;y,\uparrow,\uparrow)$	$\tilde{T}^{(d)}(x,\uparrow,\downarrow;y,\uparrow,\downarrow)$
$A52$ $B57$	$B13$ $A63$	$\frac{c}{s^2}\frac{1-y_2s^2}{x_3y_1y_2y_3(y_1,x_1)(y_1,\bar{x}_3)}$	0	$c\frac{1}{x_3y_1y_3(y_1,x_1)(y_1,\bar{x}_3)}$	0
$A26$ $B71$	$(B71)$ $(A26)$	$\frac{-s^4}{c}\frac{1}{(x_1,y_1)(\bar{x}_3,y_1)(y_3,x_3)}$	$\frac{-s^2}{c}\frac{1-x_3s^2}{x_3(x_1,y_1)(\bar{x}_3,y_1)(y_3,x_3)}$	$\frac{-s^2}{c}\frac{1-y_1s^2}{y_1(x_1,y_1)(\bar{x}_3,y_1)(y_3,x_3)}$	$\frac{-1}{c}\frac{(1-x_3s^2)(1-y_1s^2)}{x_3y_1(x_1,y_1)(\bar{x}_3,y_1)(y_3,x_3)}$
$A62$ $B17$	$(B17)$ $(A62)$	$c^3\frac{1}{x_3y_1(y_1,x_1)(y_1,\bar{x}_3)(x_3,y_3)}$	0	0	0
$A34$ $B34$	$B45$ $A45$	0	0	$\frac{c}{s^2}\frac{1}{x_1x_2x_3y_1y_3(\bar{x}_3,y_1)}$	$\frac{c^3}{s^4}\frac{1}{x_1x_2x_3y_1\bar{y}_1y_3(\bar{x}_3,y_1)}$
$A43$ $B43$	$B54$ $A54$	$\frac{-1}{s^4c}\frac{(1-x_2s^2)(1-\bar{y}_1s^2)}{x_1x_2x_3y_1\bar{y}_1y_3(y_1,\bar{x}_3)}$	$\frac{-1}{s^2c}\frac{1-\bar{y}_1s^2}{x_1x_3y_1\bar{y}_1y_3(y_1,\bar{x}_3)}$	0	0
$A35$ $B35$	$(B35)$ $(A35)$	0	0	0	$\frac{-c^3}{s^4}\frac{1}{x_1x_2x_3y_1y_2y_3(\bar{x}_3,y_1)}$
$A53$ $B53$	$(B53)$ $(A53)$	$\frac{1}{s^4c}\frac{(1-x_2s^2)(1-y_2s^2)}{x_1x_2x_3y_1y_2y_3(y_1,\bar{x}_3)}$	$\frac{1}{s^2c}\frac{1-y_2s^2}{x_1x_3y_1y_2y_3(y_1,\bar{x}_3)}$	$\frac{1}{s^2c}\frac{1-x_2s^2}{x_1x_2x_3y_1y_3(y_1,\bar{x}_3)}$	$\frac{1}{c}\frac{1}{x_1x_3y_1y_3(y_1,\bar{x}_3)}$
$A44$ $B44$	$(B44)$ $(A44)$	$\frac{-c}{s^2}\frac{y_1-\bar{x}_3}{x_1x_3\bar{x}_3y_1\bar{y}_1y_3(\bar{x}_3,y_1)}$	$\frac{-c}{s^2}\frac{1}{x_1x_3y_1\bar{y}_1y_3(\bar{x}_3,y_1)}$	$\frac{-c}{s^2}\frac{1}{x_1x_3\bar{x}_3y_1y_3(\bar{x}_3,y_1)}$	$\frac{-c^3}{s^4}\frac{1}{x_1x_3\bar{x}_3y_1\bar{y}_1y_3(\bar{x}_3,y_1)}$
$\overline{A44}$ $\overline{B44}$	$(\overline{B44})$ $(\overline{A44})$	$\frac{c}{s^4}\frac{1}{x_1x_3\bar{x}_3y_1\bar{y}_1y_3(y_1,\bar{x}_3)}$	0	0	0

Table 4: Non-zero contributions to $\tilde{T}^{(d)}(x,\uparrow,\lambda;y,\uparrow,\lambda')$ from Group C, and hence Groups D, E and F, which are obtained using the operations $\mathcal{E}$, $\mathcal{T}$ and $\mathcal{T}\circ\mathcal{E}$, respectively. In reading the middle two columns for the E and F contributions, one must keep in mind that $\mathcal{T}$ and $\mathcal{T}\circ\mathcal{E}$ interchange helicities.

d $\mathcal{E}(d)$	$\mathcal{T}(d)$ $\mathcal{T}\circ\mathcal{E}(d)$	$\tilde{T}^{(d)}(x,\uparrow,\uparrow;y,\uparrow,\uparrow)$	$\tilde{T}^{(d)}(x,\uparrow,\uparrow;y,\uparrow,\downarrow)$	$\tilde{T}^{(d)}(x,\uparrow,\downarrow;y,\uparrow,\uparrow)$	$\tilde{T}^{(d)}(x,\uparrow,\downarrow;y,\uparrow,\downarrow)$
$C12$ $D67$	$E12$ $F67$	$\frac{c}{s^4}\frac{1}{x_1\bar{x}_1^2x_2y_1\bar{y}_1y_2}$	0	0	0
$C21$ $D76$	$E21$ $F76$	0	0	$\frac{1}{s^2c}\frac{1}{\bar{x}_1^2x_2y_1\bar{y}_1y_2}$	$\frac{1}{s^4c}\frac{1-x_1s^2}{x_1\bar{x}_1^2x_2y_1\bar{y}_1y_2}$
$C17$ $D63$	$E52$ $F17$	$\frac{c}{s^2}\frac{1}{x_1\bar{x}_1x_2y_2y_3(x_1,y_1)}$	0	0	0
$C71$ $D36$	$E25$ $F71$	0	0	$\frac{1}{c}\frac{1}{\bar{x}_1x_2y_2y_3(y_1,x_1)}$	$\frac{1}{s^2c}\frac{1-x_1s^2}{x_1\bar{x}_1x_2y_2y_3(y_1,x_1)}$
$C22$ $D77$	$E11$ $F66$	$\frac{-c}{s^4}\frac{1}{\bar{x}_1^2x_2y_1\bar{y}_1^2y_2}$	0	0	0
$\overline{C22}$ $\overline{D77}$	$\overline{E11}$ $\overline{F66}$	$\frac{-1}{s^2c}\frac{1}{\bar{x}_1^2x_2\bar{y}_1^2y_2}$	0	$\frac{-1}{s^2c}\frac{1}{\bar{x}_1^2x_2y_1\bar{y}_1y_2}$	$\frac{-c}{s^4}\frac{1}{\bar{x}_1^2x_2y_1\bar{y}_1^2y_2}$
$C23$ $D74$	$E41$ $F56$	0	0	$\frac{s^2}{c}\frac{1}{x_2y_1(x_1,y_1)(y_2,\bar{x}_1)}$	$\frac{s^2}{c}\frac{1-\bar{y}_2s^2}{y_1(x_1,y_1)(y_2,x_2)(y_2,\bar{x}_1)}$
$C32$ $D47$	$E14$ $F65$	0	0	$s^2c\frac{y_2}{x_2y_1(y_1,x_1)(x_2,y_2)(\bar{x}_1,y_2)}$	0

Table 4: (cont.)

d $\mathcal{E}(d)$	$T(d)$ $T \circ \mathcal{E}(d)$	$\tilde{T}^{(d)}(x,\uparrow,\uparrow;y,\uparrow,\uparrow)$	$\tilde{T}^{(d)}(x,\uparrow,\uparrow;y,\uparrow,\downarrow)$	$\tilde{T}^{(d)}(x,\uparrow,\downarrow;y,\uparrow,\uparrow)$	$\tilde{T}^{(d)}(x,\uparrow,\downarrow;y,\uparrow,\downarrow)$
$C24$ $D75$	$E31$ $F46$	0	0	0	$c\dfrac{1-\bar{y}_2 s^2}{y_1 y_2 (x_1,y_1)(y_2,x_2)(y_2,\bar{x}_1)}$
$C42$ $D57$	$E13$ $F64$	$\dfrac{-1}{c}\dfrac{(1-y_2 s^2)^2}{y_1 y_2 (y_1,x_1)(x_2,y_2)(\bar{x}_1,y_2)}$	0	$\dfrac{-s^2}{c}\dfrac{1-y_2 s^2}{y_1 (y_1,x_1)(x_2,y_2)(\bar{x}_1,y_2)}$	0
$C25$ $D71$	$E71$ $F36$	0	0	$\dfrac{1}{c}\dfrac{1-\bar{y}_2 s^2}{x_2 y_1 y_2 (x_1,y_1)(y_2,\bar{x}_1)}$	$\dfrac{1}{s^2 c}\dfrac{(1-x_3 s^2)(1-\bar{y}_2 s^2)}{x_2 x_3 y_1 y_2 (x_1,y_1)(y_2,\bar{x}_1)}$
$C52$ $D17$	$E17$ $F63$	$\dfrac{-c}{s^2}\dfrac{1-y_2 s^2}{x_2 x_3 y_1 y_2 (y_1,x_1)(\bar{x}_1,y_2)}$	0	0	0
$C26$ $D72$	$E61$ $F26$	0	0	0	$\dfrac{-c}{s^2}\dfrac{1}{\bar{x}_1 x_2 y_1 y_2 (x_1,y_1)(y_2,\bar{x}_1)}$
$C62$ $D27$	$E16$ $F62$	$\dfrac{c}{s^2}\dfrac{1-y_2 s^2}{\bar{x}_1 x_2 y_1 y_2 (y_1,x_1)(\bar{x}_1,y_2)}$	0	$c\dfrac{1}{\bar{x}_1 x_2 y_1 (y_1,x_1)(\bar{x}_1,y_2)}$	0
$C27$ $D73$	$E51$ $F16$	$\dfrac{1}{c}\dfrac{1}{\bar{x}_1 x_2 y_2 y_3 (x_1,y_1)}$	0	$\dfrac{1}{c}\dfrac{\bar{y}_1}{\bar{x}_1 x_2 y_1 y_2 y_3 (x_1,y_1)}$	0
$C72$ $D37$	$E15$ $F61$	$\dfrac{-1}{c}\dfrac{1}{\bar{x}_1 x_2 y_1 y_2 (y_1,x_1)}$	0	$-\dfrac{1}{c}\dfrac{\bar{y}_3}{\bar{x}_1 x_2 y_1 y_2 y_3 (y_1,x_1)}$	0
$C37$ $D43$	$E54$ $F15$	0	0	$c\dfrac{y_2}{x_1 x_2 y_1 y_3 (x_2,y_2)(\bar{x}_1,y_2)}$	0

Table 4: (cont.)

d $\mathcal{E}(d)$	$\mathcal{T}(d)$ $\mathcal{T}\circ\mathcal{E}(d)$	$\tilde{T}^{(d)}(x,\uparrow,\uparrow;y,\uparrow,\uparrow)$	$\tilde{T}^{(d)}(x,\uparrow,\uparrow;y,\uparrow,\downarrow)$	$\tilde{T}^{(d)}(x,\uparrow,\downarrow;y,\uparrow,\uparrow)$	$\tilde{T}^{(d)}(x,\uparrow,\downarrow;y,\uparrow,\downarrow)$
$C73$ $D34$	$E45$ $F51$	0	0	$\frac{1}{c}\frac{1}{x_1x_2y_1y_3(y_2,\bar{x}_1)}$	$\frac{1}{c}\frac{1-\bar{y}_2s^2}{x_1y_1y_3(y_2,x_2)(y_2,\bar{x}_1)}$
$C47$ $D53$	$E53$ $F14$	$-\frac{1}{s^2c}\frac{(1-y_2s^2)^2}{x_1y_1y_2y_3(x_2,y_2)(\bar{x}_1,y_2)}$	0	$-\frac{1}{c}\frac{1-y_2s^2}{x_1y_1y_3(x_2,y_2)(\bar{x}_1,y_2)}$	0
$C74$ $D35$	$E35$ $F41$	0	0	0	$\frac{c}{s^2}\frac{1-\bar{y}_2s^2}{x_1y_1y_2y_3(y_2,x_2)(y_2,\bar{x}_1)}$
$C57$ $D13$	$E57$ $F13$	$\frac{-c}{s^4}\frac{1-y_2s^2}{x_1x_2x_3y_1y_2y_3(\bar{x}_1,y_2)}$	0	0	0
$C75$ $D31$	$E75$ $F31$	0	0	$\frac{1}{s^2c}\frac{1-\bar{y}_2s^2}{x_1x_3y_1y_2y_3(y_2,\bar{x}_1)}$	$\frac{1}{s^4c}\frac{(1-x_3s^2)(1-\bar{y}_2s^2)}{x_1x_2x_3y_1y_2y_3(y_2,\bar{x}_1)}$
$C67$ $D23$	$E56$ $F12$	$\frac{c}{s^4}\frac{1-y_2s^2}{x_1\bar{x}_1x_2y_1y_2y_3(\bar{x}_1,y_2)}$	0	$\frac{c}{s^2}\frac{1}{x_1\bar{x}_1x_2y_1y_3(\bar{x}_1,y_2)}$	0
$C76$ $D32$	$E65$ $F21$	0	0	0	$\frac{-c}{s^4}\frac{1}{x_1\bar{x}_1x_2y_1y_2y_3(y_2,\bar{x}_1)}$
$C77$ $D33$	$E55$ $F11$	$\frac{c}{s^4}\frac{1}{x_1\bar{x}_1x_2y_1y_2y_3\bar{y}_3}$	0	0	0
$\overline{C77}$ $\overline{D33}$	$\overline{E55}$ $\overline{F11}$	$\frac{1}{s^2c}\frac{1}{x_1\bar{x}_1x_2y_1y_2\bar{y}_3}$	0	$\frac{1}{s^2c}\frac{1}{x_1\bar{x}_1x_2y_1y_2y_3}$	$\frac{c}{s^4}\frac{1}{x_1\bar{x}_1x_2y_1y_2y_3\bar{y}_3}$

B Expressions for the Feynman Diagrams

Tables 3 and 4 give analytical expressions, in Feynman gauge, for the hard-scattering amplitude $\tilde{T}^{(d)}(x, \uparrow, \lambda; y, \uparrow, \lambda')$, for all non-vanishing diagrams. Diagrams are denoted by a letter, corresponding to the group in Fig. 3, and two digits, which label the segment of quark line to which the initial and final photon attaches. In the cases where both photons attach to the same segment, we denote the crossed diagram with an overbar. For example, $A51$ is the diagram with initial photon attached to the fifth segment and the final photon attached to the first segment, cf. Fig. 8.

The tabulated expressions are for a set of independent diagrams: the other can be obtained using the operations $\mathcal{E}$, $\mathcal{T}$ and $\mathcal{T} \circ \mathcal{E}$. For some diagrams d one has $(\mathcal{T} \circ \mathcal{E})(d) = d$; the redundant entry of such a diagram is in parentheses, to emphasize that it should not be counted twice. Keep in mind that, in addition to exchanging x and y, time reversal $\mathcal{T}$ exchanges initial and final photon helicities,

$$\mathcal{T}(\tilde{T}^{(d)}(x, \uparrow, \lambda; y, \uparrow, \lambda')) = \tilde{T}^{\mathcal{T}(d)}(y, \uparrow, \lambda'; x, \uparrow, \lambda). \tag{B.1}$$

In other words, $\mathcal{T}$ affects not only the contents but also the labels of the (middle two) columns.

The kinematic quantities x_i, y_i, c and s are as defined in sect. 3 and Appendix A; also $\bar{x} = 1 - x$. Finally,

$$(x, y) = x(1 - ys^2) - yc^2 \tag{B.2}$$

denotes the denominator of a potentially on-shell propagator. For brevity, we have extracted a factor of $8/s^2$, and we have omitted the $+i\varepsilon$ from each (x, y)-propagator.

C Diagram $A51$ in Detail

To illustrate our methods, this appendix presents a detailed evaluation of diagram $A51$ for the process $\gamma p \to \gamma p$. This diagram is shown with helicity and momentum assignments in Fig. 8. The internal momenta in Fig. 8 are

$$\begin{aligned} q_1 &= x_1 p - k', \\ q_2 &= x_1 p - k' - y_1 p', \\ q_3 &= (1 - x_3) p - k' - y_1 p', \\ q_4 &= y_2 p' - k, \\ q_5 &= y_3 p' - x_3 p, \end{aligned} \tag{C.1}$$

where the external momenta p, k, p' and k' have been defined in Appendix A. In Eq. (3.4) the color factor $C^{(A51)} = 4/9$; the other factors and the construction of the scattering amplitude in

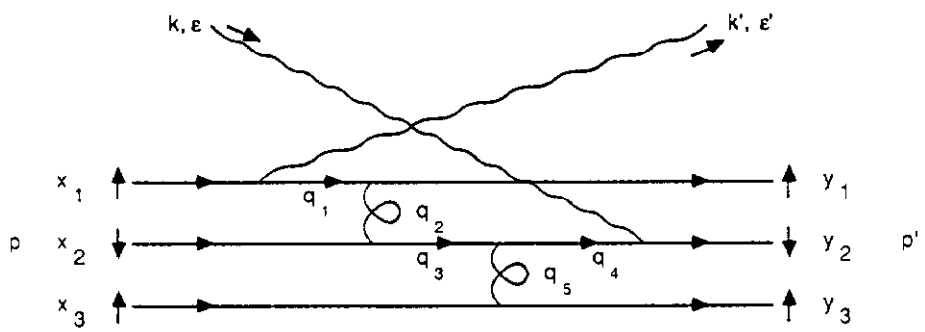

Figure 8: Diagram $A51$, which Appendix C works out in detail.

Eq. (3.3) are discussed below. For brevity, we will suppress the proton helicity $h = h' = +1$ in the factor $\tilde{T}^{(A51)}(x, h, \lambda; y, h', \lambda')$.

In the formalism of Ref. [2] the quark lines in Fig. 8 yield the following factors:

$$\begin{aligned} &\text{upper:} \quad \bar{u}_+(p')\gamma_-^\mu \not{q}_{1+} \not{\epsilon}_{f-}^* u_+(p) \\ &\text{middle:} \quad \bar{u}_-(p') \not{\epsilon}_{i+} \not{q}_{4-} \gamma_+^\nu \not{q}_{3-} \gamma_+^\mu u_-(p) \\ &\text{lower:} \quad \bar{u}_+(p')\gamma_-^\nu u_+(p) \end{aligned} \tag{C.2}$$

Performing the spinor algebra leads to an expression for the color- and flavor-independent part of the amplitude

$$\tilde{T}^{(A51)}(x, \epsilon_i; y, \epsilon_f) = \frac{\mathcal{N}}{\mathcal{D}}, \tag{C.3}$$

where

$$\mathcal{N} = -8s^3c^3s^2\left[\alpha(1 - y_2s^2) + \beta y_2 s^2\right](\gamma x_1 + \delta x_2) \tag{C.4}$$

and

$$\mathcal{D} = -s^5c^4s^2x_1x_3y_2y_3[(y_1, x_1) + i\varepsilon][(y_1, \bar{x}_3) + i\varepsilon], \tag{C.5}$$

using notation defined in Appendix A and Eq. (B.2). As in Table 3 this diagram contributes to all four combinations of photon helicity.

From Eqs. (3.3) and (3.7), the contribution of diagram $A51$ to the helicity amplitude is

$$\mathcal{M}_{\uparrow\uparrow}^{\lambda\lambda'}(s, t|A51) = (4\pi\alpha_{\rm em})(4\pi\alpha_{\rm S})^2\frac{4}{9}\left(\frac{f_{\rm N}}{8\sqrt{6}}\right)^2 \int [dx][dy]\, \tilde{T}^{(A51)}(x, \lambda; y, \lambda')\psi^{(A51)}(x, y). \tag{C.6}$$

where the coupling constants are the electromagnetic $\alpha_{\rm em}$ and the strong $\alpha_{\rm S}$, and

$$\psi^{(A51)}(x, y) = e_u^2\phi_1(x)\phi_1(y) + e_ue_d\phi_2(x)\phi_2(y) + e_ue_d\phi_3(x)\phi_3(y) \tag{C.7}$$

incorporates the distribution amplitudes and the charge factors $Z_i^{(A51)}$; the quark charges are $e_u = 2/3$ and $e_d = -1/3$. In arguments of functions x or y is an abbreviation for all three momentum fractions. The QCD-sum-rule distribution amplitudes are polynomials of the form

$$\phi(x_1, x_2, x_3) = 120x_1x_2x_3(b_0 + b_1x_1 + b_3x_3 + b_{11}x_1^2 + b_{13}x_1x_3 + b_{33}x_3^2). \tag{C.8}$$

Consequently, $\psi^{(A51)}$ is given by

$$\psi^{(A51)}(x, y) = (120)^2 \sum_{m_1, m_3, n_1, n_3} C^{(A51)}(m_1, m_3|n_1, n_3)\, x_1^{m_1+1}x_2x_3^{m_3+1}y_1^{n_1+1}y_2y_3^{n_3+1}, \tag{C.9}$$

in which the summation is limited by

$$m_1, m_3, n_1, n_3 \in \{0, 1, 2\}, \quad m_1 + m_3 \le 2, \quad n_1 + n_3 \le 2. \tag{C.10}$$

Below the obvious abbreviations m and n will be used in arguments. Clearly, if the distribution amplitude were extended to higher moments, these limits would change.

Substituting Eq. (C.9) into Eq. (C.6) yields

$$\mathcal{M}_{\uparrow\uparrow}^{\lambda\lambda'}(s, t|A51) = (4\pi\alpha_{\rm em})(4\pi\alpha_{\rm S})^2\frac{4}{9}\left(\frac{120f_{\rm N}}{8\sqrt{6}}\right)^2 \sum_{m_1, m_3, n_1, n_3} C^{(A51)}(m|n)I^{(A51)}(m, \lambda; n, \lambda') \tag{C.11}$$

where

$$I^{(A51)}(m,\lambda;n,\lambda') = \int [dx][dy]\, x_1^{m_1+1} x_2 x_3^{m_3+1} y_1^{n_1+1} y_2 y_3^{n_3+1}\, \bar{T}^{(A51)}(x,\lambda;y,\lambda'). \tag{C.12}$$

Our strategy is to work out $I^{(A51)}(m,\lambda;n,\lambda')$ using analytical and numerical techniques.

Let us concentrate on the $\lambda = \lambda' = +1$ amplitude:

$$I^{(A51)}(m,\uparrow;n,\uparrow) = \frac{1}{s^2 c} \int [dx][dy] \frac{N(x,y)}{[(y_1,x_1)+i\varepsilon]\,[(y_1,\bar{x}_3)+i\varepsilon]}, \tag{C.13}$$

where

$$N(x,y) = x_1^{m_1+1} x_2 x_3^{m_3} y_1^{n_1+1} y_3^{n_3} (1 - y_2 s^2). \tag{C.14}$$

Because the gluon with momentum q_2 and the quark with momentum q_3 can go on shell, the integral in Eq. (C.13) has an imaginary part. Using Eq. (3.16)

$$\mathrm{Re}\, I^{(A51)}(m,\uparrow;n,\uparrow) = \frac{1}{s^2 c} \int [dx][dy]\, N(x,y)\, \mathrm{P}\frac{1}{(y_1,x_1)}\, \mathrm{P}\frac{1}{(y_1,\bar{x}_3)}, \tag{C.15}$$

where P denotes the principal part, and

$$\mathrm{Im}\, I^{(A51)}(m,\uparrow;n,\uparrow) = -\frac{\pi}{s^2 c} \int [dx][dy]\, N(x,y) \left[\frac{\delta((y_1,\bar{x}_3))}{(y_1,x_1)} + \frac{\delta((y_1,x_1))}{(y_1,\bar{x}_3)} \right] \tag{C.16}$$

The six-dimensional integral in Eq. (C.15) can be reduced to a two-dimensional integral:

$$\mathrm{Re}\, I^{(A51)}(m,\uparrow;n,\uparrow) = -\frac{1}{s^2 c} \int_0^1 dx \int_0^1 dy\, \frac{B(1,n_3+1) - y s^2 B(2,n_3+1)}{1 - y s^2} \times \tag{C.17}$$

$$x^{m_3} \bar{x}^{m_1+2} y^{n_3+1} \bar{y}^{n_1+1}\, \Omega^1_{m_1+1}\left(\frac{\bar{y}}{\bar{x}(1-ys^2)} \right) \mathrm{P}\frac{1}{(x,y)},$$

which is carried out using the method [4] outlined in Appendix D. The functions

$$\Omega^n_m(a) = \int_0^1 dx\, \frac{x^m \bar{x}^n}{x - a}. \tag{C.18}$$

are special cases of the hypergeometric function. For $|a| < 1$ they can be implemented recursively:

$$\begin{aligned} \Omega^0_0(a) &= \ln|(1-a)/a|, \\ \Omega^0_m(a) &= a\Omega^0_{m-1}(a) + 1/m, \text{ and} \\ \Omega^n_m(a) &= (1-a)\Omega^{n-1}_m(a) - B(m+1,n); \end{aligned} \tag{C.19}$$

for $|a| > 1$ they can be implemented using the Gauss hypergeometric series [21].

The imaginary part can be reduced to a one-dimensional integral:

$$\mathrm{Im}\, I^{(A51)}(m,\uparrow;n,\uparrow) = -\frac{\pi}{s^2 c}(H_1 + H_2), \tag{C.20}$$

where

$$H_1 = c^{2n_1} B(m_1+2,1) B(1,n_3+1) \int_0^1 dx\, \frac{x^{m_1+n_1+3} \bar{x}^{m_3+n_3+1}}{(1-xs^2)^{n_1+n_3+2}} \left[1 - \frac{s^2}{n_3+2} \frac{\bar{x}}{1-xs^2} \right] \tag{C.21}$$

and

$$H_2 = -c^{2n_1} B(1,m_3+1) B(1,n_3+1) \int_0^1 dx\, \frac{x^{m_1+n_1+2} \bar{x}^{m_3+n_3+2}}{(1-xs^2)^{n_1+n_3+2}} \left[1 - \frac{s^2}{n_3+2} \frac{\bar{x}}{1-xs^2} \right]. \tag{C.22}$$

These integrals can be reduced to the hypergeometric function and evaluated numerically without resorting to Monte Carlo integration.

Our results for $\mathcal{M}^{\uparrow\uparrow}_{\uparrow\uparrow}(A51)$ are tabulated in Table 5, using the CZ distribution amplitude [11]. The error estimates for the real part are those reported by VEGAS.

Table 5: The contribution of diagram $A51$ to the helicity amplitude $\mathcal{M}^{\uparrow\uparrow}_{\uparrow\uparrow}$. The energy dependence has been factored out, but the factors preceding the integral in Eq. (C.6) have been included. We have set $\alpha_{\rm em}^{-1} = 137.036$, $\alpha_{\rm S} = 0.3$, and $f_{\rm N} = 5.2 \times 10^{-3}$ GeV^2.

θ	$10^3 s^2 \times \mathrm{Re}[\mathcal{M}^{\uparrow\uparrow}_{\uparrow\uparrow}(A51)]$	$10^3 s^2 \times \mathrm{Im}[\mathcal{M}^{\uparrow\uparrow}_{\uparrow\uparrow}(A51)]$
20°	−1.020(1)	0.180···
30°	−1.084(1)	0.156···
40°	−1.177(1)	0.115···
50°	−1.307(1)	0.049···
60°	−1.484(1)	−0.055···
70°	−1.716(1)	−0.219···
80°	−2.021(2)	−0.482···
90°	−2.412(2)	−0.908···
100°	−2.890(2)	−1.614···
110°	−3.448(3)	−2.813···
120°	−3.944(4)	−4.911···
130°	−3.912(5)	−8.696···
140°	−1.550(11)	−15.675···
150°	9.565(28)	−28.134···
160°	57.041(72)	−42.216···

D Monte Carlo Integration of Integrals Defined by Principal Part Prescription

All principal part integrals encountered on this work take the form of Eq. (3.17). Considering the ξ integration, the pole appears at $\eta c^2/(1-\eta s^2)$, i.e. parametrized by η. Hence, it is enough to illustrate the folding method in one dimension, i.e. for integrals of the form:

$$J = \int_0^1 dx\, \mathrm{P}\, \frac{f(x)}{x-a}, \quad 0 < a < 1, \quad f(a) \neq 0. \tag{D.1}$$

The principal part prescription is defined by

$$J = \lim_{\varepsilon \to 0} (J_1 + J_2) \tag{D.2}$$

where

$$J_1 = \int_0^{a-\varepsilon} dx \frac{f(x)}{x-a}, \quad J_2 = \int_{a+\varepsilon}^1 dx \frac{f(x)}{x-a}. \tag{D.3}$$

In each integral we change variables:

$$y_1 = \frac{x}{a} \;\Rightarrow\; J_1 = \int_0^{1-\varepsilon/a} dy_1 \mathcal{J}_1(y_1), \quad \mathcal{J}_1(y) = \frac{f(ay)}{y-1} \tag{D.4}$$

and

$$y_2 = \frac{a(1-x)}{a^2 + (1-2a)x} \;\Rightarrow\; J_2 = \int_0^{1-\varepsilon/a} dy_2 \mathcal{J}_2(y_2), \quad \mathcal{J}_2(y) = \frac{(1-a) f(a(1-ay)/d)}{d(1-y)}, \tag{D.5}$$

where $d = a + (1-2a)y$. The integration variables y_1 and y_2 satisfy

$$\left.\frac{dx}{dy_1}\right|_{y_1=1} = -\left.\frac{dx}{dy_2}\right|_{y_2=1} \tag{D.6}$$

and hence the upper limits in Eqs. (D.4) and (D.5) approach 1 uniformly, up to negligible terms of order ε^2 in the upper limit of the latter. Combining Eqs. (D.2), (D.4) and (D.5) yields an expression in which the limit $\varepsilon \to 0$ may be taken. The result,

$$J = \int_0^1 dy\,[\mathcal{J}_1(y) + \mathcal{J}_2(y)], \tag{D.7}$$

contains no singularities, and VEGAS [3] has no difficulty evaluating it. The remote danger that the random number generator chooses the value $y = 1$, for which $\mathcal{J}_1$ and $\mathcal{J}_2$ are individually infinite, will be reported by the computer.

This method can be extended to higher dimensional integrals and to cases where there is more than one pole in the integrand [4]. Reference [4] also discusses the need for a correction term $f(a)\ln|(1-a)/a|$ for changes of variable that do not satisfy Eq. (D.6).

Reference [9] regulates poles by using the Feynman $i\varepsilon$ prescription in the computer program. The principal part in Eq. (3.16) is replaced by two large peaks of opposite sign, and the δ-function is replaced by a narrow Lorentzian. A stable result is sought for a sequence of small values of ε, which controls the width of the peaks. In an example from pion Compton scattering that can be integrated analytically, the $i\varepsilon$ method, with $\varepsilon = 0.005$, can be off by as much as 5% for the real part and 10% for the imaginary part, while the reported statistical errors are less by one tenth. (Our method agrees with the exact result, within the reported errors.) In the more complicated expressions for nucleon Compton scattering, the discrepancies in the $i\varepsilon$ method are larger. We used it to (try to) compute the contribution of diagram $A51$ to the $\lambda = \lambda' = +1$ helicity amplitude (cf. Appendix C). Using over 75,000 function calls and 10 iterations, the imaginary part, as a function of scattering angle, did not even resemble the correct result.

References

[1] G.P. Lepage and S.J. Brodsky, *Phys. Rev.* **D22**, 2157 (1980)

[2] G.R. Farrar and F. Neri, *Phys. Lett.* **B130**, 109 (1983)

[3] G.P. Lepage, *J. Comp. Phys.* **27**, 192 (1978)

[4] B. Nižić, *Phys. Rev.* **D35**, 80 (1987)

[5] M.A. Shupe, et al, *Phys. Rev.* **D19**, 1921 (1979)

[6] M. Jung, et al, *Z. Phys.* **C10**, 197 (1981)

[7] J. Duda, et al, *Z. Phys.* **C17**, 319 (1983)

[8] T. Ishii, et al, *Nucl. Phys.* **B254**, 458 (1985);
Y. Wada, et al, *Nucl. Phys.* **B247**, 313 (1984)

[9] G.R. Farrar and H. Zhang, *Phys. Rev.* **D41**, 3348 (1990); (Erratum) **D42**, 2413 (1990)

[10] G. Martinelli and C.T. Sachrajda, *Phys. Lett.* **B217**, 319 (1989)

[11] V.L. Chernyak and A.R. Zhitnitsky, *Nucl. Phys.* **B246**, 52 (1984)

[12] I.R. Zhitnitskiĭ, A.A. Oglobin and V.L. Chernyak, *Yad. Fiz.* **48**, 841 (1988) [*Sov. J. Nucl. Phys.* **48**, 536 (1988)];
V.L. Chernyak and I.R. Zhitnitsky, *Z. Phys.* **C42**, 569 (1989)

[13] I.D. King and C.T. Sachrajda, *Nucl. Phys.* **B297**, 785 (1987)

[14] M. Gari and N.G. Stefanis, *Phys. Lett.* **B175**, 462 (1986); *Phys. Rev.* **D35**, 1074 (1987)

[15] E. Maina and G.R. Farrar, *Phys. Lett.* **B206**, 120 (1988)

[16] We learned about this point, and its importance, from Stan Brodsky and Peter Lepage (private communication, 1984).

[17] G.R. Farrar, G. Sterman and H. Zhang, *Phys. Rev. Lett.* **62**, 2229 (1989)

[18] S.J. Brodsky and G.R. Farrar, *Phys. Rev. Lett.* **31**, 1153 (1973); *Phys. Rev.* **D11**, 1309 (1975)

[19] G.R. Farrar, K. Huleihel and H. Zhang, *Nucl. Phys.* **B349**, 655 (1991)

[20] A. Messiah, *Quantum Mechanics* (John Wiley and Sons, New York), p. 1032

[21] M. Abramowitz and I.A. Stegun, *Handbook of Mathematical Functions* (Dover, New York)